AWARD NUMBER: W81XWH-12-1-0291

TITLE: Targeting Midbodies in Ovarian Cancer Stem Cells as a Therapeutic Strategy.

PRINCIPAL INVESTIGATOR: Stephen Doxsey

Contracting Organization: Universtiy of Massachusetts
Worcester, MA 01605

REPORT DATE: October 2013

TYPE OF REPORT: Annual

PREPARED FOR: U.S. Army Medical Research and Materiel Command
Fort Detrick, Maryland 21702-5012

# REPORT DOCUMENTATION PAGE

*Form Approved*
**OMB No. 0704-0188**



| 1. REPORT DATE *(DD-MM-YYYY)* | 2. REPORT TYPE | 3. DATES COVERED *(From - To)* |
|---|---|---|
| October 2013 | Annual | 30September2012–29September2013 |

**4. TITLE AND SUBTITLE**
Targeting Midbodies in Ovarian Cancer Stem Cells as a Therapeutic Strategy.

**5a. CONTRACT NUMBER**

**5b. GRANT NUMBER**
W81XWH-12-1-0291

**5c. PROGRAM ELEMENT NUMBER**

**6. AUTHOR(S)**
Stephen Doxsey

email:stephen.doxsey@umassmed.edu

**5d. PROJECT NUMBER**

**5e. TASK NUMBER**

**5f. WORK UNIT NUMBER**

**7. PERFORMING ORGANIZATION NAME(S) AND ADDRESS(ES)**
Universtiy of Massachusetts
Medical School
373 Plantation Street, Suite 210
Worcester, MA 01605

**8. PERFORMING ORGANIZATION REPORT NUMBER**

**9. SPONSORING/MONITORING AGENCY NAME(S) AND ADDRESS(ES)**
U.S. Army Medical Research and Materiel Command
Fort Detrick, Maryland
21702-5012

**10. SPONSOR/MONITOR'S ACRONYM(S)**

**11. SPONSORING/MONITORING AGENCY REPORT NUMBER**

**12. DISTRIBUTION AVAILABILITY STATEMENT**
Approved for public release; distribution unlimited

**13. SUPPLEMENTARY NOTES**

**14. ABSTRACT**
The etiology and early events in the development and progression of ovarian tumorigenesis are among the least understood of all human malignancies. A major difficulty in the treatment of ovarian cancer is tumor recurrence and chemoresistance. One explanation for these impediments to a cure for ovarian cancer is that a subset of cancer cells, called 'cancer stem cells (CSCs)' or 'cancer initiating cells (CICs)', is both the source of ovarian cancer and the major contributor to the refractory nature of ovarian cancer to chemotherapeutic challenge [4-7]. For these reasons, a better understanding of ovarian cancer stem cells and their contribution to ovarian cancer is essential and may provide the best strategy to ameliorate this disease. In the last decade, the cancer stem cell theory has been supported by many studies and has become an attractive hypothesis for the generation and propagation of human cancers. Putative ovarian CSCs have been identified in mouse and human and used to successfully induce tumor formation and serial tumor propagation in mice. However, there has been limited success in therapeutic targeting of CSCs for ovarian tumor eradication.

**15. SUBJECT TERMS**
ovarian cancer, stem cells, midbody, mitosis, microtubules

| 16. SECURITY CLASSIFICATION OF: | | | 17. LIMITATION OF ABSTRACT | 18. NUMBER OF PAGES | 19a. NAME OF RESPONSIBLE PERSON |
|---|---|---|---|---|---|
| a. REPORT | b. ABSTRACT | c. THIS PAGE | U | 37 | USAMRMC |
| U | U | U | | | 19b. TELEPONE NUMBER (*Include area code)* |

## TABLE OF CONTENTS

**Introduction…… 4**

**Body……. 4-5**

**Key Research Accomplishments……5**

**Reportable Outcomes……5-7**

**Conclusion……7**

**References. ……...7**

**Appendices……none**

**INTRODUCTION.**

Ovarian cancer is a disease of uncontrolled cell division. Cell division normally creates two genetically identical daughter cells through severing of a cytoplasmic bridge that interconnects them. The midbody is an organelle within the bridge that is involved in severing. Previously, midbodies were thought to be lost from cells after division, but we show they can be retained, accumulated and increased with tumor grade. The long-term goal of this project is to identify putative MB-containing ovarian cancer cells and target them for chemotherapeutic elimination of ovarian cancer. This proposal is designed to test this idea. We will determine if MBs are present in putative ovarian cancer stem cells (CSCs) from multiple ovarian cancer cell lines and tumor types (Task 1), isolate MB-containing ovarian cancer cells and directly test them for tumorigenic potential in mice (Task 2) and determine if degradation of MBs in ovarian cancer cells diminishes or eliminates their tumorigenic potential (Task 3).

**BODY**

***Task 1. Test whether MBs are present in ovarian CSCs in vitro and in vivo.***

Isolate ovarian CSCs from cell lines and test for enrichment of MBs. We have successfully isolated putative ovarian CSCs from two cell lines SKOV3 and OVCA) using 2 different methods: a) We isolated the side population of SKOV3 cells based on their ability to use the ABC transporter to pump out the DNA dye Hoechst 33342 (the so called side population or SP). b). We also isolated putative CSCs through detection of fluorescent-tagged cell surface CSC markers (CD133+, CD44+, CD117+). (Dyall et al., 2010; Ponnusamy et al., 2008).

In both strategies, putative CSCs were fixed, spun onto coverslips and stained for MBs using two different and effective MB markers, MKLP1 (Fig. 1) and MgcRacGAP. There was near complete (98.8+/-0.3%) concordance in MB staining using these markers. In both CSC preparations MBs were found to be significantly higher in the CSC fraction **(**Fig. 2, SP). We are testing other ovarian cancer cell types.

As expected, we also found that MBs were present in ovarian tumors and preliminary results indicate that MBs increase with increasing ovarian tumor grade.

During these analyses, we unexpectedly discovered that a large number of canonical ovarian oncogenes and tumor suppressors localized to MBs in epithelial ovarian cancer cells. These include HER-2/neu, c-myc and K-ras, p53 (Fig. 4), BRCA1, BRCA2 and others. This result provides a potential molecular mechanism for the tumorigenic property of MBs and could serve as a novel therapeutic method for treating ovarian cancer. We will not follow up on this result, but rather, we will attempt to garner additional funding to study this new discovery.

***Task 2. Test the tumorigenic potential of MBs***.

We tested MB+ cells isolated based on MB fluorescence (MKLP-1-GFP) and flow cytometry for growth in soft agar. We observed a dramatic increase in soft agar growth. Once we complete the in vitro assays, we will begin testing tumor induction in mice.

We next tested another method of increasing MBs. We prevented their receptor-mediated degradation by depleting the autophagy receptor, NBR1. shRNA depletion of NBR1 blocked autophagic degradation of MBs and increased the percent of MB+ cells. This was accompanied by an increase in soft agar growth by percentages similar to those observed for cells isolated by MKLP-GPF, above. During the course of this work, we discovered another autophagy protein, NipSnip2. It had an enhanced effect on MB degradation when depleted compared to NBR1.

**Task 3.** ***Test if specific targeting of MBs for autophagic degradation is a therapeutic strategy for ovarian cancer.***
We showed that NBR1-GFP expression accelerated autophagy-mediated degradation of MBs in ovarian cancer cells (SKOV3, Fig. 5; OVCA, not shown). Under these conditions, soft agar colony number (a measure of ovarian tumor potential) was dramatically decreased (preliminary results, Fig. 5). This result has important implications for ovarian tumor therapy.

We also showed that NipSnip2 expression dramatically increases MB degradation leading to decreased tumor potential. It is more efficacious than NBR1 in this regard (not shown, ~7-fold).

**SUMMARY OF KEY RESEARCH ACCOMPLISHMENTS:**

1. Midbodies are inherited by one daughter cell and accumulate in ovarian cancer cells (Fig. 1).
2. Midbodies are in ovarian cancer stem cells (Fig. 2).
3. The presence of midbodies is associated with increased in vitro tumor potential over MB-negative ovarian cancer cells (preliminary data, Fig. 3).
4. Midbodies serve as scaffolds for anchoring ovarian cancer oncogenes, tumor suppressors and cancer stem cell proteins (Fig. 4).
5. NBR1 expression effectively eliminates ovarian cancer cells in vitro (Fig. 5). In vivo studies ongoing.

**REPORTABLE OUTCOMES (**The following are outcomes of this study)**:**

**Manuscripts related to this study.** These papers focus on aspects of cell division including midbody inheritance and degradation and are related, directly or indirectly, to findings discussed in this report.

1. Hehnly and Doxsey, The Centrosome Regulates the Rab11- Dependent Recycling Endosome Pathway at Appendages of the Mother Centriole. Current Biol. 20: 1944-50, 2012. ***Highlighted in Nature Reviews Molecular Cell Biology.***
2. Hehnly H, Doxsey S. Rab11 endosomes contribute to mitotic spindle orientation. *Developmental Cell* 28, 497-507, 2014. ***See Commentary in Dev Cell 28, 480-482.***
3. Chen CT, Ettinger AW, Huttner WB, Doxsey SJ. Resurrecting remnants: the lives of post-mitotic midbodies Trends in Cell Biology 23, 118-28 2013.

**Cell lines.**

We established SKOV3 and OVCA cell lines expressing GFP-MKLP1, which targets midbodies (Fig. 1).
We established SKOV3 cell lines expressing GFP-Cep55, which targets to midbodies (not shown).
We established SKOV3 cell lines expressing GFP-NBR1, which targets to autophagosomes (not shown).
We established SKOV3 cell lines expressing GFP-NipSnip2, which targets autophagosomes (not shown).

**Funding opportunities.**

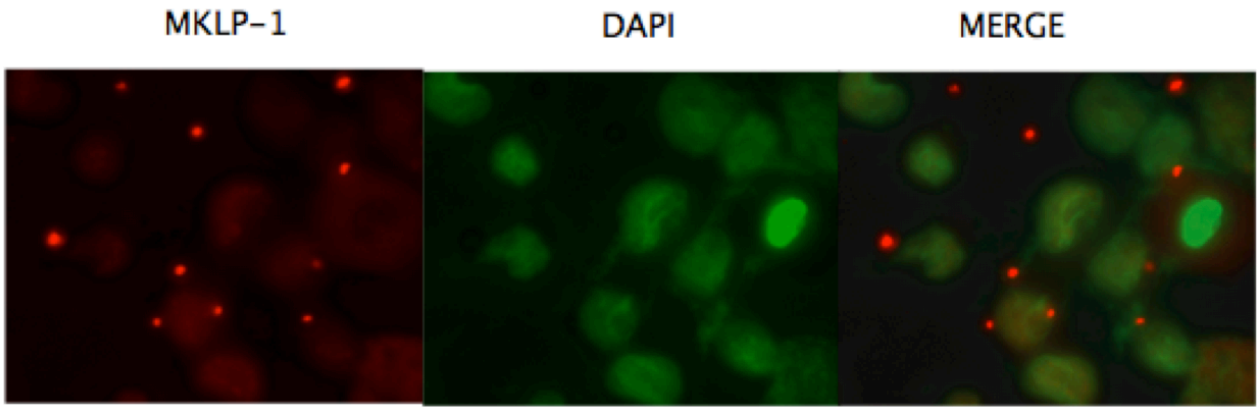


**Fig. 1.** Midbodies (GFP-MKLP-1, left) accumulate in ovarian cancer cells, right and merge (SKOV).

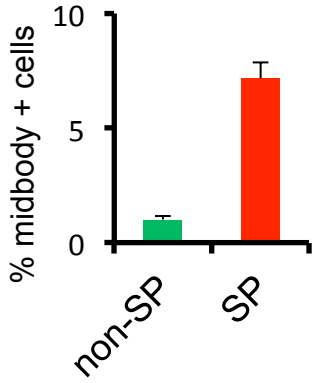


**Fig. 2.** SKOV cell side population (SP,cancer stem cells) show significantly more midbody positive cells than non-SP. X-axis, % midbody-positive cells

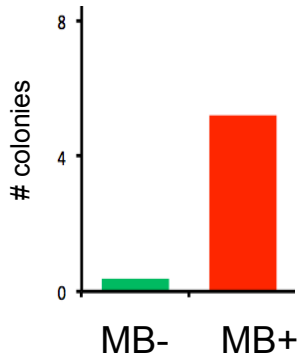


**Fig. 3.** Tumor potential of SKOV cells (soft agar colonies in vitro). MB-, midbody-negative cells. MB+, midbody –positive cells.

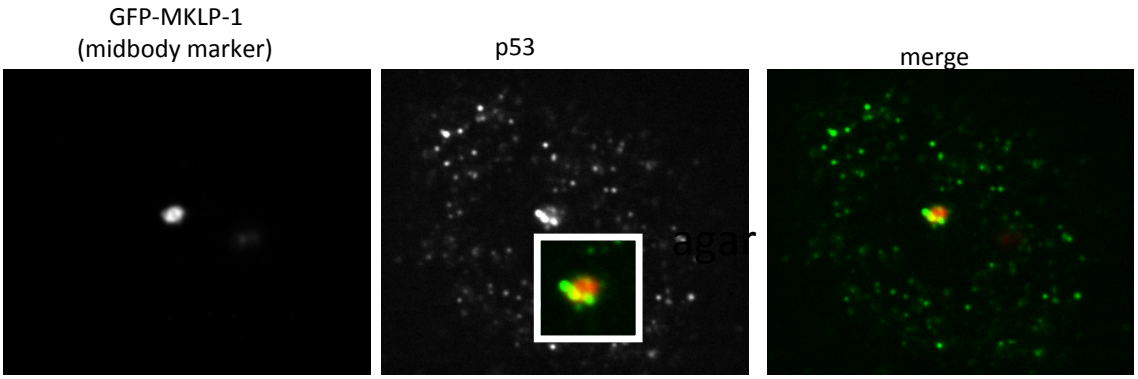


**Fig. 4.** Midbody-positive cells (GFP-MKLP-1 ) are associated with the ovarian cancer cancer tumor suppressor, p53. SKOV cell line expressing midbody marker (GFP-MKLP-1, left panel) and stained for p53 (center panel). Merge (right panel).

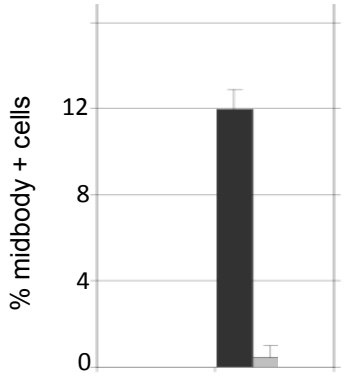


**Fig. 5.** NBR1-GFP expressing cells have significantly fewer midbodies than GFP expressing cells.

A postdoctoral fellow in my laboratory (Dr. Heidi Hehnly) was awarded a K99 grant from NIH based, in part, on the findings of this study.

Based on this work, I applied for a Breakthrough award from the Department of Defense.

**Invited seminars based on work in this project, which was initiated in Sept. 2012.**

**2012**

| | |
|---|---|
| 10/2012 | **Plenary Lecture and Teaching Lectures** Kisumu Medical Training College, Kisumu, Kenya, East Africa |
| 11/2012 | International Drug Discovery Science/Technology, Nanjing China |
| 12/2012 | American Society of Cell Biology, San Francisco, CA |

**2013**

| | |
|---|---|
| 01/2013 | **Plenary Lecture,** Asian Clinical Congress, Bangkok, Thailand |
| 03/2013 | "Building a Centrosome" Workshop, West Sussex, U.K. |
| 05/2013 | University of Algarve, Portugal |
| 05/2013 | University of Toronto, Toronto Canada |
| 11/2013 | "Anti-Cancer Drugs", Stockholm, Sweden |
| 12/2013 | "Anti-cancer Drugs "Moscow Russia" |
| 12/2013 | "Biological and Biomedical Sciences" Dar-Es-Salaam, Tanzania |

**2014 (invited and expected to attend)**

| | |
|---|---|
| 03/2014 | UPenn |
| 04/2014 | Univ. Tennessee |
| 09/2014 | "Midbodies as a target for cancer therapy", Athens, Greece |
| 11/2014 | "Midbodies as a target for cancer therapy", PepCon, Dalian, China |

**CONCLUSION:**

The results reported in this funding period show promise toward ovarian cancer therapies. Several lines of investigation suggest this can be done: MBs enhance ovarian cancer whereas decreasing MBs kills ovarian cancer cells. Overexpression of autophagy proteins (NBR1, NIPSNIP2) decreases MBs and kills ovarian cancer cells. MB-positive ovarian cancer cells appear to be ovarian cancer stem cells. This suggests that MB targeting for ovarian cancer therapy will target the cell that is the most insidious of all ovarian cancer cells, the ovarian stem cell. In turn, MB+ ovarian cancer stem cells are likely to be the cells that are drug resistant, recurrent and form metastatic lesions, all of which have been the most difficult to treat. The finding that MBs anchor ovarian cancer oncogenes, tumor suppressors and cancer stem cell proteins suggests that they may serve as scaffolds for ovarian tumor pathways. We expect the work will ultimately have a sustained and significant impact on ovarian cancer for a number of additional reasons: We provide a new understanding of ovarian cancer etiology, namely the finding that an organelle never before associated with cancer may in fact be a key player in ovarian tumor development and progression. We also believe that we have identified a new and effective ovarian cancer stem cell identification strategy based on a novel and atypical biomarker, the MB. We believe that our laboratory is the only one in the world working in this area of cancer biology.

**REFERENCES**

*Kuo et al., Midbody accumulation through evasion of autophagy contributes to cellular reprogramming and tumorigenicity. Nature Cell Biology 13: 1467, 2011.
*Dyall et al., Cancer stem cells and epithelial ovarian cancer. J Oncology 1-9, 2010.
*Ponnusamy et al., Ovarian cancer: Emerging concept on cancer stem cells. J Ovarian Res 86, 1-9, 2008

Developmental Cell
Article

# Rab11 Endosomes Contribute to Mitotic Spindle Organization and Orientation

Heidi Hehnly[1] and Stephen Doxsey[1,*]
[1]Program in Molecular Medicine, University of Massachusetts Medical School, Worcester, MA 01605, USA
*Correspondence: stephen.doxsey@umassmed.edu
http://dx.doi.org/10.1016/j.devcel.2014.01.014

## SUMMARY

**During interphase, Rab11-GTPase-containing endosomes recycle endocytic cargo. However, little is known about Rab11 endosomes in mitosis. Here, we show that Rab11 localizes to the mitotic spindle and regulates dynein-dependent endosome localization at poles. We found that mitotic recycling endosomes bind γ-TuRC components and associate with tubulin in vitro. Rab11 depletion or dominant-negative Rab11 expression disrupts astral microtubules, delays mitosis, and redistributes spindle pole proteins. Reciprocally, constitutively active Rab11 increases astral microtubules, restores γ-tubulin spindle pole localization, and generates robust spindles. This suggests a role for Rab11 activity in spindle pole maturation during mitosis. Rab11 depletion causes misorientation of the mitotic spindle and the plane of cell division. These findings suggest a molecular mechanism for the organization of astral microtubules and the mitotic spindle through Rab11-dependent control of spindle pole assembly and function. We propose that Rab11 and its associated endosomes cocontribute to these processes through retrograde transport to poles by dynein.**

## INTRODUCTION

We recently showed that the recycling endosome (RE) GTPase, Rab11, binds to mother centriole appendages in interphase cells. RE vesicles interact with and organize around these appendages. Endosome dissociation from centrosomes disrupts endosome recycling (Hehnly et al., 2012). We hypothesized that REs may, in turn, play a role in centrosome function. In fact, Rab11 was identified in a screen for mitotic regulators of microtubule (MT) dynamics in *Caenorhabditis elegans* (Zhang et al., 2008) and was shown to require dynein for this function (Ai et al., 2009). Rab11 is also an important regulator of endosome asymmetric distribution in sensory organ precursor (SOP) cells during cell division (Emery et al., 2005). Rab11-vesicles have recently been implicated in asymmetric spindle positioning in mouse oocytes (Holubcová et al., 2013), but how Rab11-vesicles can directly contribute to this process was not thoroughly investigated. However, the authors do propose that these vesicles function as cytoskeletal modulators (Holubcová et al., 2013). Here, we explore possible functions for Rab11 in the formation of spindle poles, assembly of MT nucleating, MT anchoring, and regulatory proteins at poles, organization of astral MTs, and orientation of mitotic spindles and the plane of cell division.

## RESULTS

### Rab11-Associated Endosomes Associate with Mitotic Spindle Poles and the Mitotic Spindle

Little is known of Rab11 and endosome function during spindle formation in mitosis. We found that GFP-Rab11-decorated-endosomes and the Rab11 effector, FIP3, clustered at spindle poles and along the mitotic spindle (Figures 1A and 1B; Figure S1A available online; Movies S1 and S2) (noted in Hobdy-Henderson et al., 2003 and Takatsu et al., 2013). Rab11 also localized to isolated spindle poles demonstrating that it is a bona fide centrosome protein (Figure S1D). In cells that were cold treated (Figure 1C), which destabilizes dynamic microtubules while preserving kinetochore MTs (Meunier and Vernos, 2011), Rab11 localized predominantly to kinetochore MTs (Figure 1C). This suggested that Rab11-associated endosomes were bound to MTs and that they might possibly be transported along spindle fibers to and from the pole. We established that these Rab11 endosomes were, in fact, recycling endosomes by staining for several additional RE proteins (Figures 1A–1C, 2A, and 2B). However, the early endosome Rab5 effector, EEA1, and Golgi complex proteins did not localize to these organelles (Figures 2C and S2B; Movie S2) (Golgi positioning reviewed in Yadav and Linstedt, 2011).

The selective mitotic MT localization of Rab11 and its associated endosomes (Figures 1A–1C and S1A) was confirmed by biochemical assessment of microtubule pellets (Figure S1B). Mitotic MTs bound significantly more Rab11 than interphase MTs due most likely to degradation of the Rab11 GTPase activating protein (GAP), Evi5, which converts Rab11 to its GDP-binding state (Laflamme et al., 2012; Dabbeekeh et al., 2007; Eldridge et al., 2006) (Figure S1B). Consistent with the MT association and GTP status of Rab11, was the observation that forced expression of constitutively active Rab11(Q70L) increased MT-association over dominant-negative Rab11(S25N) (Figure S1C). This suggested that the enhanced MT-association of mitotic Rab11 could result from reduced Evi5 levels (Eldridge et al., 2006) (Figures 1A and S1B) subsequently causing an increase in active Rab11.

### REs Contain MT-Nucleating Components and Dynein

To better understand the differences between endosomes in mitotic versus interphase cells, we examined the molecular

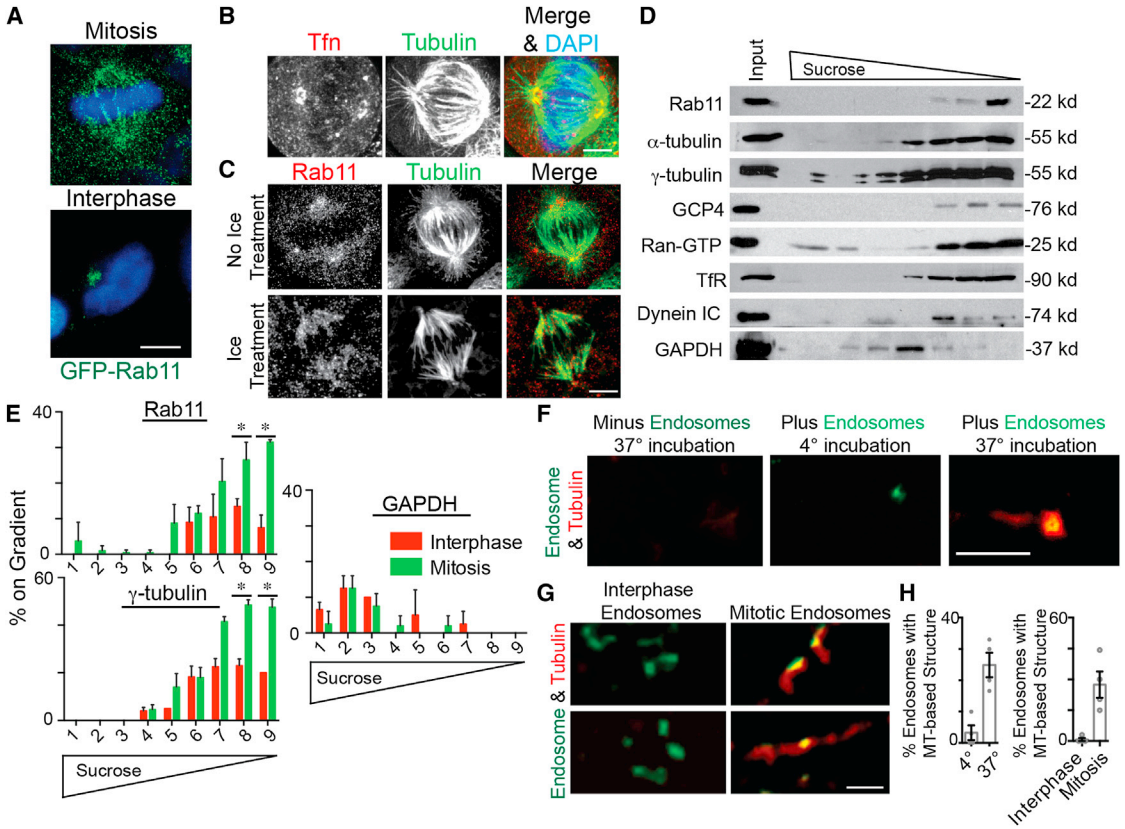


**Figure 1. Recycling Endosomes Localize along the Spindle, Contain γ-Tubulin, and Associate with an MT-Based Structure**

(A) Cells expressing GFP-Rab11 were fixed during mitosis or interphase to visualize Rab11. DAPI, blue. Scale bar, 5 μm.

(B and C) Alexa Fluor 594-Tfn filled endosomes (B; red) and Rab11 (C; red) localize to the mitotic spindle and spindle poles. MTs, green; DAPI, blue. Scale bars, 5 μm. In cold-treated cells that maintain stable kinetochore-attached-MTs, Rab11 localized to MTs (C).

(D) Immunoblots of endosomes were isolated by floatation in a sucrose gradient and labeled for transferrin receptor (TfR) and Rab11. Endosomes cofractionated with the centrosome proteins α- and γ-tubulin, GCP4, Ran-GTP, and dynein intermediate chain (IC), but not with the cytosolic component GAPDH.

(E) Mitotic and interphase endosomes isolated by floatation were analyzed for associated Rab11, γ-tubulin, and GAPDH. Mitotic endosomes contained significantly more Rab11 and γ-tubulin than interphase endosomes (n = 3 experiments). *p < 0.01; for representative immunoblot, see Figure S1E.

(F) Tubulin (10 μM) was incubated with or without isolated mitotic endosomes (green, decorated with GFP-FIP3), spun onto coverslips, and tested for MT association. Endosomes showed MT association at 37°C, but not 4°C. Tubulin alone did not form an MT-based structure without endosomes present. Scale bar, 3 μm.

(G) Isolated mitotic versus interphase endosomes (GFP-FIP3, green) were spun onto coverslips and tested for MT association/assembly (tubulin, red). Two examples are shown for each. Scale bar, 3 μm.

(H) The percent of endosomes forming MT-based structures was quantified. Left: 25% of mitotic endosomes formed MT-structures at 37°C, compared to ~4% at 4°C (n = 3 experiments, p < 0.01). Right: 25% of mitotic endosomes formed MT-based structures compared to 0% in control (n = 4 experiments, p < 0.01). See also Figure S1 and Movie S1.

composition of isolated endosomes. Endosomes detected by the presence of GFP-FIP3, a Rab11 effector that localizes to spindle poles, and Rab11 itself (Figure S1A), were isolated via flotation upward through a sucrose step gradient (Ori-McKenney et al., 2012) (Figure 1D). Biochemical analysis of the mitotic endosomes revealed proteins involved in MT organization (e.g., dynein) as well as MT nucleation, spindle pole organization, and regulators of these processes (e.g., γ-tubulin, α-tubulin, GCP4, Ran-GTP) (Figure 1D). The specificity of spindle pole proteins localization to endosomes was confirmed by showing that GAPDH did not cofractionate with endosomes (Figures 1D and S1E). The presence of α-tubulin in these isolated endosome fractions (Figure 1D) is consistent with Rab11 pelleting in MT pull-down experiments (Figure S1B).

We found that isolated mitotic endosomes contained significantly more Rab11 and γ-tubulin than interphase endosomes (Figures 1E and S1E). Notably, mitotic endosomes are enriched at mitotic spindle poles/centrosomes compared to interphase endosomes (Tfn-filled) (Movie S1). This suggested that mitotic membranes may recruit more MT-nucleating components, which is consistent with their potential role in centrosome maturation. To directly address this, we tested MT nucleation from isolated mitotic and interphase endosomes, as done for Golgi vesicle MT nucleation assays in previous studies (Ori-McKenney et al., 2012). Similar to Golgi MT nucleation, ~25% of mitotic endosomes assembled linear MT elements, which were not present at 4°C (Figures 1F and 1H) or when nocodazole was added (Figure S1F). Endosomes isolated from

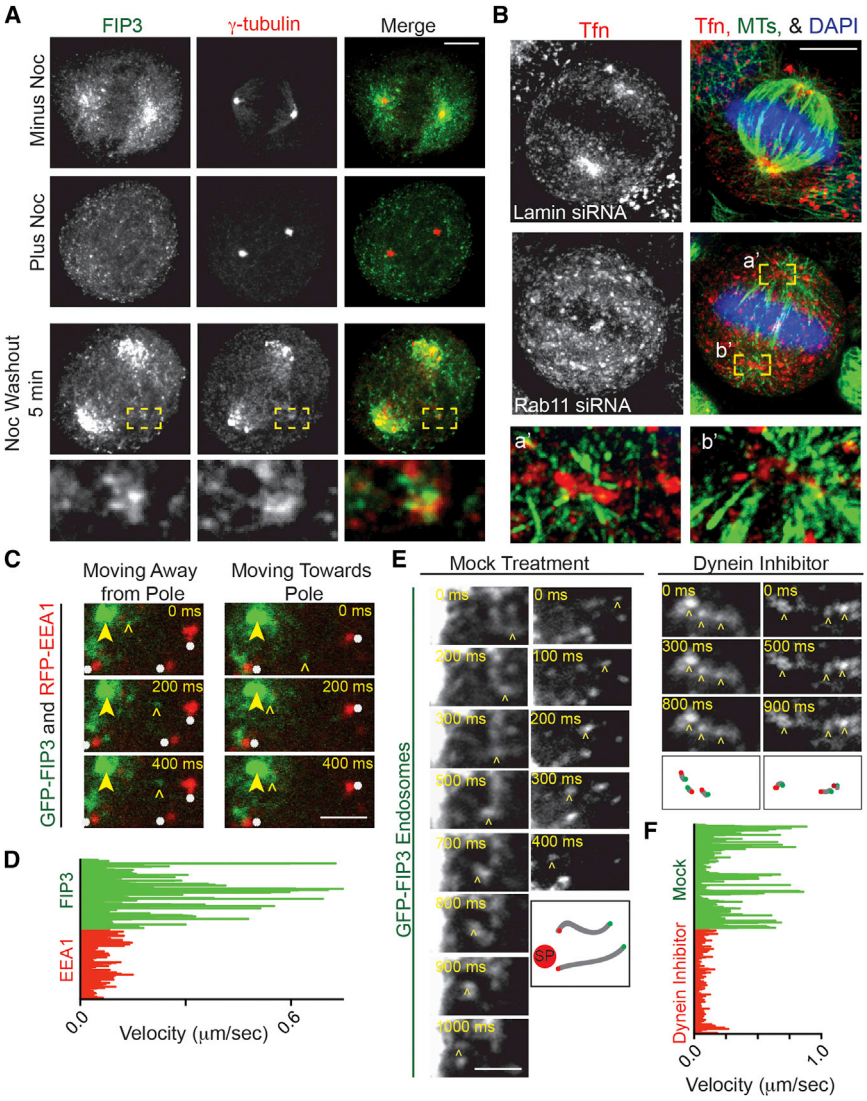


**Figure 2. Recycling Endosomes Exhibit Rab11-Dependent Spindle Pole Localization and Dynein-Mediated Transport**

(A) Maximum projections of mitotic cells after nocodazole or mock treatment and 5 min after nocodazole washout. Cells were fixed, stained for γ-tubulin (red) and FIP3 (green). Mock-treated cells show FIP3 having spindle and pole localization, whereas nocodazole-mediated MT disruption dispersed FIP3 from poles. Five minutes after nocodazole washout, FIP3 refocuses at the spindle pole and at acentrosomal foci (inset, labeled with γ-tubulin, red).

(B) Control (lamin siRNA) and Rab11-depleted cells incubated with Alexa Fluor 594-conjugated Tfn (red) to label endosomes. Most endosomes focus around poles (MTs; green) in control cells, but are dispersed in Rab11-depleted cells. DAPI, blue. MT organization around poles was also disrupted after Rab11 depletion (insets a′, b′, disrupted endosomes with MTs, 5× original image). Scale bar, 5 μm.

(C) Selected images from time-lapse movies of GFP-FIP3-labeled REs (marked by open arrowhead) moving toward and away from spindle poles (spindle pole marked by closed arrowhead) and dispersed RFP-EEA1 early endosomes remaining fairly immobile (marked by white asterisk). Scale bar, 1 μm. See also Movie S2.

(D) GFP-FIP3- and RFP-EEA1-decorated endosome track velocities were characterized. RFP-EEA1 tracks moved at a decreased velocity compared to GFP-FIP3 tracks ($n > 30$ tracks in $n = 3$ cells for each condition).

(E) Selected still images from time-lapse movies of GFP-FIP3-labeled REs moving toward spindle poles in prometaphase cells. Left: a mock control (DMSO only) prometaphase cell showing minus-end directed motion of FIP3-decorated RE toward pole (marked by open arrowhead; Movie S3). Right: a dynein-inhibited (Firestone et al., 2012) prometaphase cell with no minus-end mediated transport occurring (endosomes marked by open arrowhead). Schematic representation of shown puncta is depicted below time course. Green point represents when the vesicle starts moving, red point is when it stopped, and gray line is the path it took. Red circle labeled "SP" depicts where spindle pole is. Scale bar, 1 μm.

(F) GFP-FIP3-decorated recycling endosome tracks were characterized in either a control or a dynein inhibitor-treated prometaphase cell. The dynein inhibitor significantly decreased GFP-FIP3 endosome velocity ($n > 40$ measured tracks for each treatment, three cells measured per treatment).

See also Figure S2 and Movies S2 and S3.

interphase cells showed little to no detectable MT nucleation (Figures 1G and 1H).

## Depletion of Rab11 or FIP3 Disrupts Endosome Organization at Spindle Poles

To further test the mechanism of endosome localization to spindle poles, we depleted Rab11 or FIP3 using previously characterized siRNAs (Hehnly et al., 2012) (Figure S2C). In both cases, the association of REs with spindle pole (Figures 2B, S2B, and S2C) was decreased ~3-fold compared with controls. Depolymerization of MTs similarly decreased spindle pole localization of REs (Figures 2A, 2B, and S2A) demonstrating a requirement for MTs in organization or MT-dependent transport of endosomes.

## REs Require Dynein-Based Transport for Spindle Pole Localization

To more directly distinguish between (1) binding of REs to spindle poles via MTs at this site, or (2) transport of REs to spindle poles via MTs, RE dynamics (TfR in Figure S2A; GFP-FIP3 in Figures 2A and 2C–2F; Tfn-filled in Movie S1) were examined in living cells or in fixed cells over a time course. After spindle MTs were disrupted by nocodazole, spindle reassembly was imaged over a time course after drug washout. Spindle reassembly in control cells was initiated by renucleation of MTs from spindle poles and reorganization of endosomes around the poles. We found that endosomes reorganized around acentrosomal peripheral microtubule clusters containing γ-tubulin (Figure 2A, modeled in Figure 3B) that formed in the cytoplasm and moved

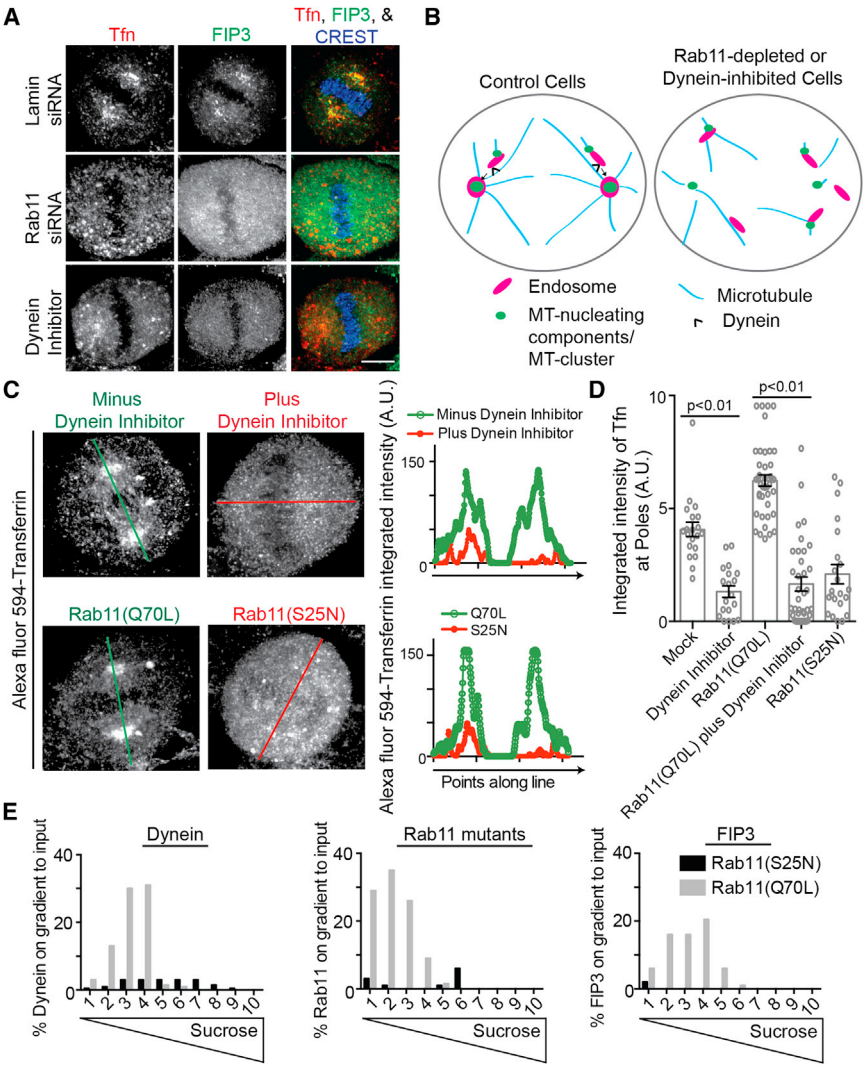


**Figure 3. Rab11 and Dynein Coordinately Organize Recycling Endosomes at Mitotic Spindle Poles**

(A) Cells treated with a dynein inhibitor (Firestone et al., 2012), or depleted of lamin (control) or Rab11 were incubated with Alexa Fluor 594-conjugated Tfn (red) to label endosomes. Mitotic cell maximum projections are shown, and cells were stained for the Rab11-effector FIP3 (green) specifically labeling REs. REs were dispersed with dynein inhibition and Rab11 depletion. Scale bar, 5 μm.

(B) Model depicting REs together with MT clusters contributing to spindle organization and function by acting as a carrier to transport spindle pole components to spindle poles by dynein-mediated transport. RE transport to the spindle pole is disrupted by either dynein inhibition or Rab11 depletion.

(C) Cells treated with dynein inhibitor or expressed Rab11(S25N) had significantly less Alexa Fluor 594-conjugated Tfn (red) labeled endosomes organized at mitotic spindle poles compared to either a mock control (DMSO-treated) or cells expressing Rab11(Q70L). Scale bar, 5 μm. A line scan through the mitotic spindle poles (oriented by γ-tubulin staining, not shown) is drawn and the integrated intensity is plotted for Tfn.

(D) Shown is quantification of Tfn intensity at spindle poles (n = 25 poles per treatment, p values marked on graph; representative of n = 3 experiments). A significant increase in spindle pole localized Tfn was observed in cells expressing Rab11(Q70L) when compared to Rab11(S25N). However, Rab11(Q70L) did not cause an increase in Tfn in the presence of a dynein inhibitor.

(E) Endosomes isolated by floatation from cells expressing Rab11(S25N) or Rab11(Q70L) were compared for amounts of bound Rab11, dynein, and FIP3. Mitotic endosomes containing Rab11(Q70L) recruited significantly more dynein and the Rab11-effector FIP3 than membranes isolated from cells expressing Rab11(S25N), (representative of n = 3 experiments, e.g., representative western blots shown in Figure S3B). See also Figure S3.

vectorially to spindle poles (Figures 2A and S2A). These observations suggested that endosomes were being transported on spindle MTs as part of these MT clusters (Figures 2A and S2A; modeled in Figure 3B), to become incorporated into spindle poles. In our previous work, we showed that these MT clusters carried centrosome proteins to spindle poles (Delaval et al., 2011). Consistent with this notion is the observation that the MT clusters in this study appear to be transporting endosomes that we show contain centrosome proteins identified in our biochemical assays (Figure 1D, colocalization between FIP3 and γ-tubulin in Figure 2A).

We contend that endosomes are part of the MT cluster-based transport pathway, as REs recruit the same/similar centrosome proteins and move to spindle poles. Work on MT clusters suggests that dynein may be the driving force for this process (Delaval et al., 2011; Tulu et al., 2003). To directly test the role of dynein in endosome movements, we examined the dynamics of GFP-FIP3-labeled REs in mitotic cells. We observed movement toward and away from the mitotic spindle poles (Figure 2C; Movies S2 and S3). Endosomes moving toward the spindle pole had an average velocity of 0.8 μm/s (Figure 2E; Movie S3). REs were more motile than RFP-EEA1-labeled early endosomes, which rarely organized at poles or moved in a poleward direction (Figures 2C and 2D; Movies S2 and S3). To test the role of dynein in these movements, we acutely inactivated the motor with a specific membrane-permeable dynein inhibitor (Firestone et al., 2012). This essentially abolished vectorial retrograde motion of the GFP-FIP3 REs (Figures 2E and 2F).

## Rab11 Regulates Endosome Organization at Mitotic Spindle Poles through Dynein

To further analyze the role of Rab11 and dynein in recycling endosome organization, we either depleted Rab11, expressed a dominant-negative Rab11 mutant, Rab11(S25N), expressed a constitutive-active mutant, Rab11(Q70L), and/or treated cells with a dynein inhibitor. We discovered that when Rab11 activity was inhibited by either depletion or Rab11(S25N) expression, the spindle pole localization of REs was disrupted (Tfn-loaded, FIP3-labeled)

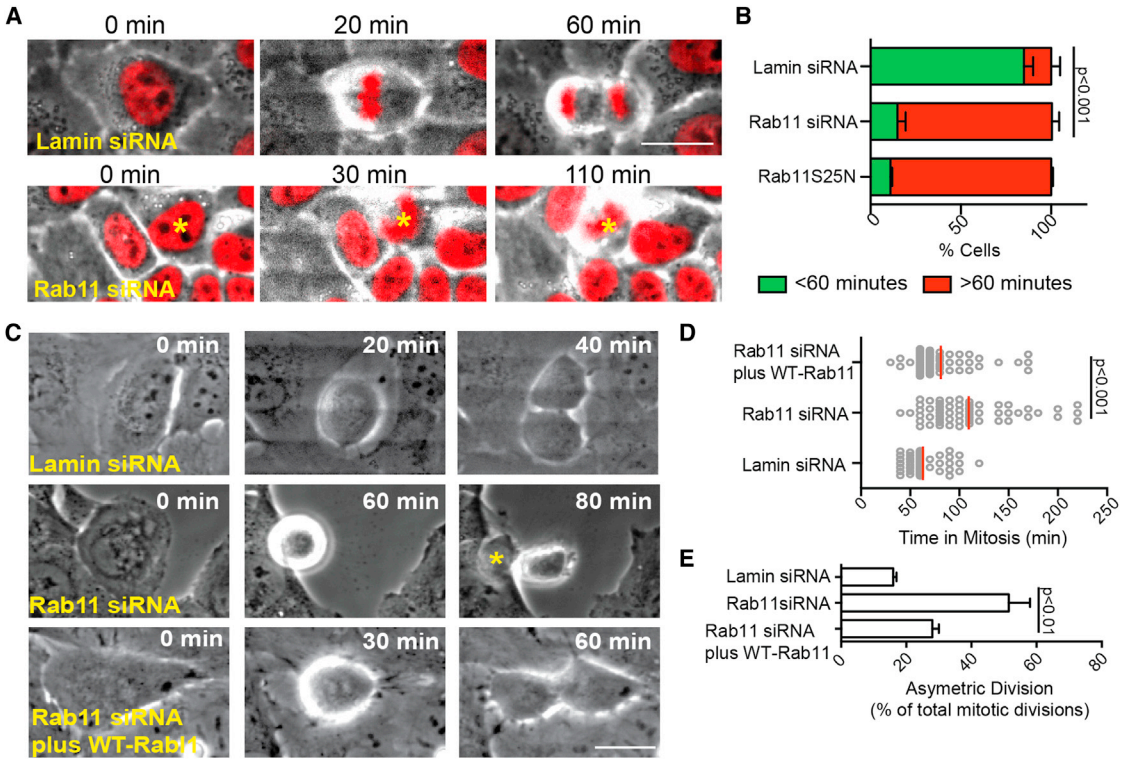


**Figure 4. Rab11 Plays a Role in Mitotic Progression**

(A) Time-lapse imaging show Rab11-depleted HeLa cells stably expressing histone 2B RFP (H2B, red), entering mitosis as in control (lamin siRNA). However, Rab11-depleted cells become delayed in prometa/metaphase. Scale bar, 20 μm. See also Movie S4.

(B) Quantification of cells that spent >60 min or <60 min in mitosis following lamin (control) or Rab11 depletion, or after expression of dominant-negative (S25N) Rab11 (~5-fold decrease in <60 min, n > 3 experiments; $p < 0.001$ between lamin siRNA and Rab11 siRNA).

(C and D) Rab11-depleted cells spent more time in mitosis (2-fold, n > 75 cells, representative of n = 3 experiments, p value depicted on graph) compared with lamin (control). The increased time spent in mitosis and asymmetric divisions can be rescued by an RNAi-resistant Rab11 construct. Scale bar, 20 μm.

(E) Asymmetric division, determined by cell flattening is increased in Rab11-depleted cells. $p < 0.001$, n = 3 experiments, asterisk indicating daughter cell that flattened first (C).

See also Figure S4 and Movie S4.

(Figures 2B, S2B, 3A–3D, and S3A; modeled in Figure 3B). Similar results were obtained with the dynein inhibitor (Figures 3A–3C). In contrast, expression of constitutive-active Rab11(Q70L) induced tighter organization of endosomes at spindle poles (Figures 3C and S3A), and in some cases fewer endosomes were observed along the mitotic spindle (compare minus dynein inhibition to Rab11(Q70L) expression in images and line scan of Figure 3C).

Based on these findings, we hypothesized that Rab11 recruited dynein to mitotic endosome membranes. To test this, we assessed whether Rab11(Q70L) could rescue endosome organization at mitotic spindle poles when dynein was inhibited. First, we showed that Rab11(Q70L) expression increased spindle pole-associated endosomes (Figure 3C; quantification in Figure 3D). We next determined that endosomes in cells expressing Rab11(Q70L) and treated with a dynein inhibitor (Firestone et al., 2012) were decreased to the same level as treatment alone (Figures 3C and 3D), suggesting that active-Rab11 recruits dynein to mitotic endosomes. To address this more directly, we examined mitotic endosomes isolated from cells expressing either Rab11(Q70L) or Rab11(S25N) (Figures 3E and S3B). Endosomes from cells expressing constitutive-active Rab11(Q70L) recruited Rab11(Q70L) and dynein but those from cells expressing dominant-negative Rab11(S25N) recruited neither Rab11(S25N) nor dynein. As a positive control, Rab11(Q70L) recruited its effector, FIP3, to mitotic membranes where Rab11(S25N) did not (Figures 3E and S3B). These results suggest that active-Rab11 assists in dynein recruitment to endosomes during mitosis (Figures 3B and 3E).

## Rab11 Is Involved in Mitotic Progression

During the course of these studies, we noticed that the prevalence of mitotic cells was increased when Rab11 activity was disrupted. To formally address the origin of this phenotype, we performed time-lapse imaging to determine the time spent in mitosis in cells depleted of Rab11 or expressing dominant-negative Rab11 (Rab11(S25N) (HeLa cells in Figures 4A and 4B; U2OS cells in Figures 4C–4E, S4A, and S4B). Cells were engineered to express histone 2B-RFP (H2B) (Figure 4A; Movie S4) to identify chromosome organization and mitotic stage. Eighty percent of control cells (Figure 4B) or 60% of Rab11-depleted cells rescued by expression of a siRNA-resistant Rab11 (Figures 4D and S2C) progressed into anaphase within 60 min. In contrast, only ~20% of Rab11-depleted or Rab11(S25N)-expressing cells entered anaphase within this time frame (average

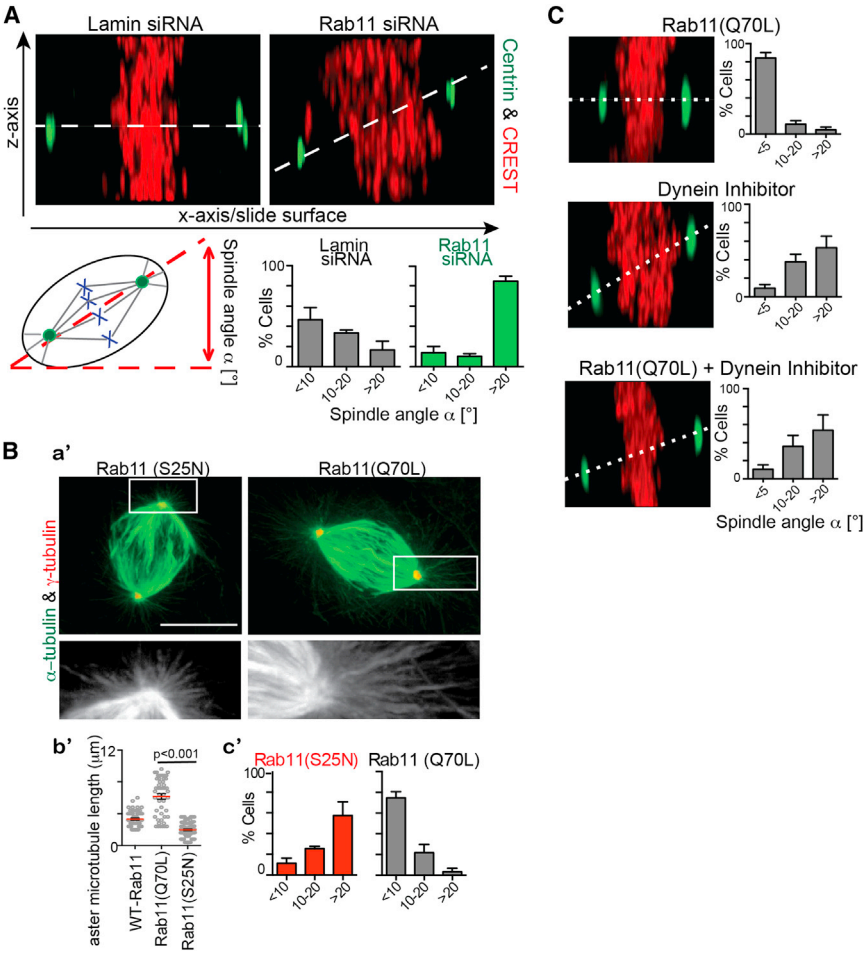


**Figure 5. Rab11 Is Involved in Orientation of the Mitotic Spindle**

(A) Top: Rab11 depletion showed increased asymmetric divisions by measuring spindle angle (dotted line) relative to substrate (maximum projection of the z axis, centrin [green], and kinetochores [CREST, red]). Bottom: quantification showing a significant increase (>20°) of spindle angle in cells depleted of Rab11 (~2-fold, n = 3 experiments, $p < 0.001$ comparing spindle angles >20° across treatments. n > 20 cells counted/experiment).

(B) Longer astral MTs in constitutively active Rab11(Q70L)-expressing cells compared to dominant-negative Rab11(S25N)-expressing cells revealed by staining for α-tubulin (green; a′). Shown is quantification of astral MT length (n > 50 asters per treatment, $p < 0.001$; b′). Quantification showing a significant increase (>20°) of spindle angle in cells expressing Rab11(S25N) compared to Rab11(Q70L) (n = 3 experiments; n > 20 cells counted/experiment; c′).

(C) Z axis maximum projections of a cell expressing Rab11(Q70L) and/or incubated with a dynein inhibitor (n = 3 experiments. n > 20 cells counted/experiment).

100–130 min; Figures 4B–4D and S4B). This mitotic delay was confirmed by imaging live cells stably expressing cyclin B-GFP to distinguish prometaphase from metaphase cells. As expected, cyclin B levels in control cells were highest in metaphase and decreased sharply at anaphase onset (Lindqvist et al., 2009; Chen et al., 2012). In contrast, cyclin B levels in Rab11-depleted cells (Figure S4C) remained elevated for prolonged time periods, demonstrating a metaphase delay.

## Rab11 Plays a Role in Spindle Orientation

The mitotic delay following Rab11 disruption suggested a defect in mitotic spindle organization and indicated that the GTPase may have additional mitotic functions. Closer inspection of mitotic spindles in Rab11-depleted cells revealed several defects in spindle organization and function. The most prevalent phenotype was misorientation of the mitotic spindle and the plane of cell division. More specifically, the spindle angle relative to the cell-substrate adhesion plane in ~60% of Rab11-depleted cells was >20°, whereas most control spindles were parallel to the substratum (~80%) (Figure 5A). In addition, we found that the cell division plane was oriented more vertically in Rab11-depleted cells compared to control cells where the division plane was horizontal to the substratum (Figure 4C). The misoriented division plane caused a delay in flattening of the daughter cell farthest away from the substrate (Figure 4C; quantification in Figure 4E). To determine the cellular and molecular basis of spindle and cell division misorientation, we examined spindles in more detail.

## Rab11 Plays a Role in Astral MT Organization

Astral MT arrays in cells depleted of Rab11 (data not shown) or expressing dominant-negative Rab11(S25N) were disrupted when compared to wild-type or constitutively-active Rab11(Q70L)-expressing cells (Figure 5B). This was consistent with the increased spindle angle in either Rab11-depleted cells (Figure 5A) or Rab11(S25N)-expressing cells (Figure 5B). Constitutively active Rab11(Q70L) enhanced astral MT networks, substantiating the importance of the GTPase state of Rab11 in the formation of the astral MT network, which is the subpopulation of spindle MTs involved in contacting dynein at the cell cortex and mediating spindle reorientation through dynein motor activity (Kotak and Gönczy, 2013). Consistent with this is our finding that dynein inhibition causes an increased spindle angle similar to Rab11-depleted cells (Figure 5C). Constitutively active Rab11(Q70L) could not rescue the spindle asymmetry phenotypes observed under dynein inhibition (Figure 5C) compatible with dynein and Rab11 coordinately regulating symmetric division.

## Cell and Molecular Mechanism of Spindle Defects following Rab11 Depletion

The localization of Rab11 to spindle poles and spindle MTs (Figures 1 and S1) and its role in mitotic progression and spindle assembly (Figures 4 and 5) suggested a role for the GTPase in spindle pole assembly and function. Rab11 depletion (Figures 6A–6D and S2C) or dominant-negative Rab11(S25N) expression (Figure 6E) decreased spindle pole levels of major PCM proteins (γ-tubulin and pericentrin), MT-anchoring and plus-end binding

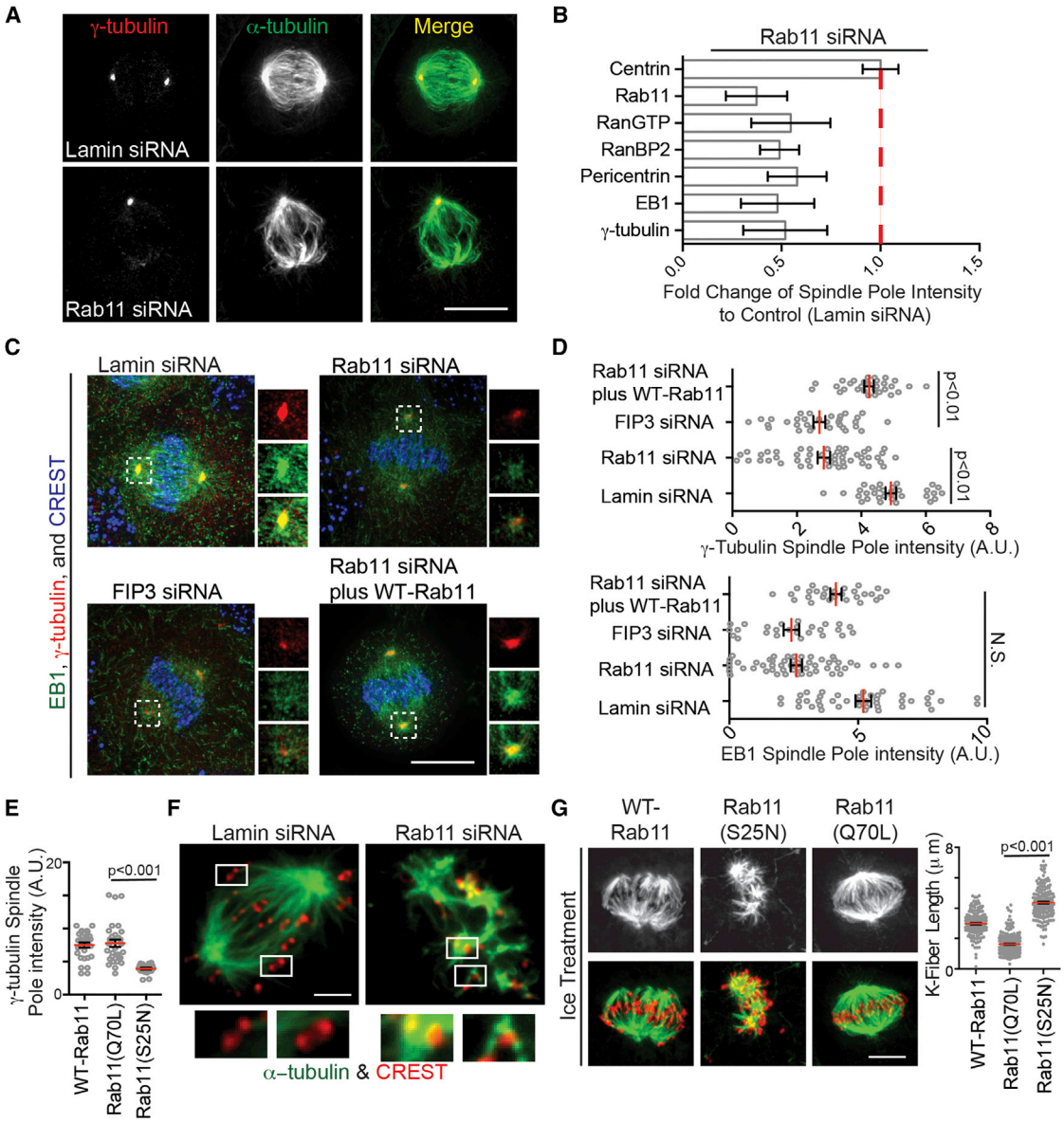


**Figure 6. Rab11 Contributes to the Organization of the Mitotic Spindle**

(A) Control or Rab11-depleted metaphase cells were stained for γ-tubulin (red) and MTs (green). Scale bar, 10 μm.

(B) Loss of spindle pole proteins as indicated in Rab11-depleted cells was quantified (n = 3 experiments). Fold change was calculated over control (lamin siRNA). A significant loss of γ-tubulin, EB1, RanBP2, RanGTP, and pericentrin was observed in Rab11-depleted cells (n = 3; $p < 0.001$).

(C) Cells were depleted of lamin, FIP3, Rab11, or Rab11 complimented with siRNA-resistant Rab11. Metaphase cells were stained for γ-tubulin (red), EB1 (green), and CREST (blue). Scale bar, 10 μm.

(D) Spindle pole-associated γ-tubulin and EB1 were decreased in Rab11- and FIP3-depleted cells, but not in control cells (lamin siRNA) or cells treated with Rab11-siRNA rescued with an siRNA-resistant Rab11 vector (n > 25 poles per treatment; p values depicted on graphs). N.S., not significant.

(E) A significant increase in γ-tubulin at spindle poles was observed in cells expressing Rab11(Q70L) when compared to Rab11(S25N) (n = 25 poles per treatment; $p < 0.001$).

(F) Control prometaphase cells 5 min after nocodazole washout had robust MT-growth (green) from poles, whereas Rab11-depleted cells had a significant number of MT clusters emanating from kinetochores (CREST, red) and little from poles (data not shown). Insets show kinetochores with MT clusters in Rab11-depleted cells compared to none in control. Scale bar, 3 μm.

(G) Kinetochore fibers in cells expressing WT-Rab11, Rab11(S25N), and Rab11(Q70L) after cold treatment, fixation, and staining with anti-α-tubulin (MTs, green) and kinetochores (CREST, red). Scale bar, 3 μm. Right: quantification of kinetochore fiber disruption following Rab11(S25N) expression. (n > 100 K-fibers per treatment; p value depicted on graph).

See also Figure S5.

proteins (EB1), and MT nucleation regulators (Ran-GTP and its binding protein RanBP2), (~2-fold) (Figures 6A–6E and S5A). It is important to reiterate that most of these proteins are, at least in part, bound to endosomes (Figure 1). Equally important was the observation that spindle pole levels of the centriolar protein centrin (Figure 5A) and the MT-motor, Kif2a (Figure S5B) were not affected by Rab11 depletion. These results demonstrate a role for Rab11 in the organization of a selective subset of spindle pole proteins, primarily those involved in centrosome maturation, the process of centrosome protein recruitment initiated during progression into mitosis and completed by metaphase (Mahen and Venkitaraman, 2012). This rapid recruitment of centrosome proteins drives a dramatic increase in MT-nucleating activity (Bornens, 2012).

To further examine the role of Rab11 in centrosome maturation, we performed a functional test monitoring both assembly of centrosome proteins onto spindle poles and spindle-pole-mediated MT-nucleating activity over time. Spindles were disassembled with nocodazole, then examined at different times after nocodazole washout for protein recruitment and MT nucleation (Delaval et al., 2011) (Figure S5C). At 1 min of regrowth, spindle poles in control cells showed an increased ability to nucleate MTs and recruit the spindle pole proteins γ-tubulin, pericentrin, and EB1 (Figure S5C). These activities were impaired in Rab11-depleted cells (Figure S5C). At 5 min of regrowth, control cells nucleated MTs robustly from the poles. In contrast, Rab11-depleted cells showed little nucleation at poles. Instead, MT clusters assembled at kinetochores (Figure 6F). This finding suggests that spindle poles in Rab11-depleted cells are compromised in their ability to nucleate MTs thus allowing the kinetochore-mediated MT-formation pathway to be activated or dominant. In control cells, when spindle poles are intact, no kinetochore MTs are generated. This result also demonstrates that kinetochores are intact and functional in Rab11-depleted cells and are not likely candidates for chromosome misalignment. Eventually after 40 min, spindles were assembled with noncongressed chromosomes whereas control spindles had tight metaphase plates (Figure S5D). It is important to note that the kinetochore-based process of spindle assembly in Rab11-depleted cells is similar to that in acentrosomal cells (Theurkauf and Hawley, 1992), where spindle MTs grow from sites around kinetochores then self-organize into a spindle (Heald et al., 1996; Theurkauf and Hawley, 1992). Based on these findings and our live-cell video microscopy (Figure 2), we conclude that Rab11 and its associated endosomes assist in spindle pole function by organizing MT-nucleating components at this site (Figure 6).

To more closely examine kinetochore fiber integrity, we employed cold treatment to specifically eliminate dynamic MTs from mitotic cells (Meunier and Vernos, 2011; Firestone et al., 2012). Kinetochore fibers in control cells were well organized and robust (Figures 6G and S5E). Following Rab11 depletion or dominant-negative Rab11(S25N) expression, kinetochore fibers were reduced to collections of small disorganized linear segments (Figures 6G and S5E). These results support the idea that Rab11-depleted spindle poles are compromised in MT nucleation and MT anchoring and likely release MTs as observed (Figures 6G and S5E). Finally expression of constitutively active Rab11(Q70L) generated longer kinetochore-based MTs than cells expressing WT-Rab11 or Rab11(S25N) (Figure 6G). These results demonstrate that the GTP state of Rab11 is important for spindle pole-mediated MT nucleation and anchoring.

### Rab11 Is Involved in Chromosome Alignment

In addition to spindle misorientation, Rab11-depleted cells showed a significant increase in misaligned chromosomes (~60%) (Figure S6A). Chromosome congression and alignment requires both attachment of chromosomes to MTs and tension on the chromosomes. It is important to note that tension on chromosomes requires robust MT attachments, not only at kinetochores but also at spindle poles. MT attachment to poles is an integral, but often unappreciated, part of the spindle assembly process. We propose that disruption of spindle poles and spindle pole generated MTs in Rab11-depleted cells (Figure 6) disrupts chromosome attachments to spindle pole MTs (Figure 7). Consistent with this are results showing that kinetochores are not compromised by Rab11 depletion as they can induce MT formation (Figure 6F) and activate the spindle assembly checkpoint (SAC) (Figure 7). These compromised MT attachments at spindle poles could prevent the generation of tension at the chromosomes and thus activate the SAC. In fact, our data show that the SAC is activated, as Mad1, ZW10, and BubR1 remained at kinetochores in Rab11-depleted cells. There was no change in the kinetochore kinesin, MCAK (Figures 7A and 7B), suggesting that the kinetochores were structurally intact. We further found a significant increase in dynein localization to kinetochores in Rab11-depleted cells (Figure S6B).

We propose a model for chromosome alignment that is controlled by Rab11. First, kinetochores in Rab11-depleted cells are functional in that they are able to activate SAC and generate and bind to MTs. It is unlikely that they are the cause of SAC activation. In contrast, spindle pole MT nucleation and anchoring are disrupted, which can prevent or compromise MT spindle pole attachments, (perhaps through the MT-nucleating protein γ-tubulin). This, in turn, could activate the SAC through the inability to maintain tension at spindle poles. In fact, diminished tension was revealed as a dramatic reduction in interkinetochore distances (Figure 7C) and the presence of Aurora B at kinetochores flanked by two CREST-labeled puncta (Figure 7D), where it senses tension (Howell et al., 2004; Famulski and Chan, 2007; Lampson and Cheeseman, 2011).

## DISCUSSION

This work has led us to unexpected functions of the Rab11 GTPase and its associated endosomes. First, our results provide evidence for Rab11 function in the construction of spindle poles. We propose that this occurs through dynein-mediated transport of endosomes that, in turn, carries MT nucleating/anchoring and regulatory proteins to the poles. In essence, Rab11 endosomes act as carriers to recruit and organize MT-nucleating material at spindle poles through dynein (Figures 1, 2, and 3). We believe that this is particularly significant because previous studies suggested that endosomes, like Golgi complexes and endoplasmic reticulum disperse throughout the cytoplasm during mitosis, and membrane trafficking is thought to be halted until cytokinesis (Foley and Kapoor, 2013; Yadav and Linstedt, 2011; Chen et al., 2012). Second, when Rab11 is disrupted, the molecular and functional integrity of spindle poles is compromised. This

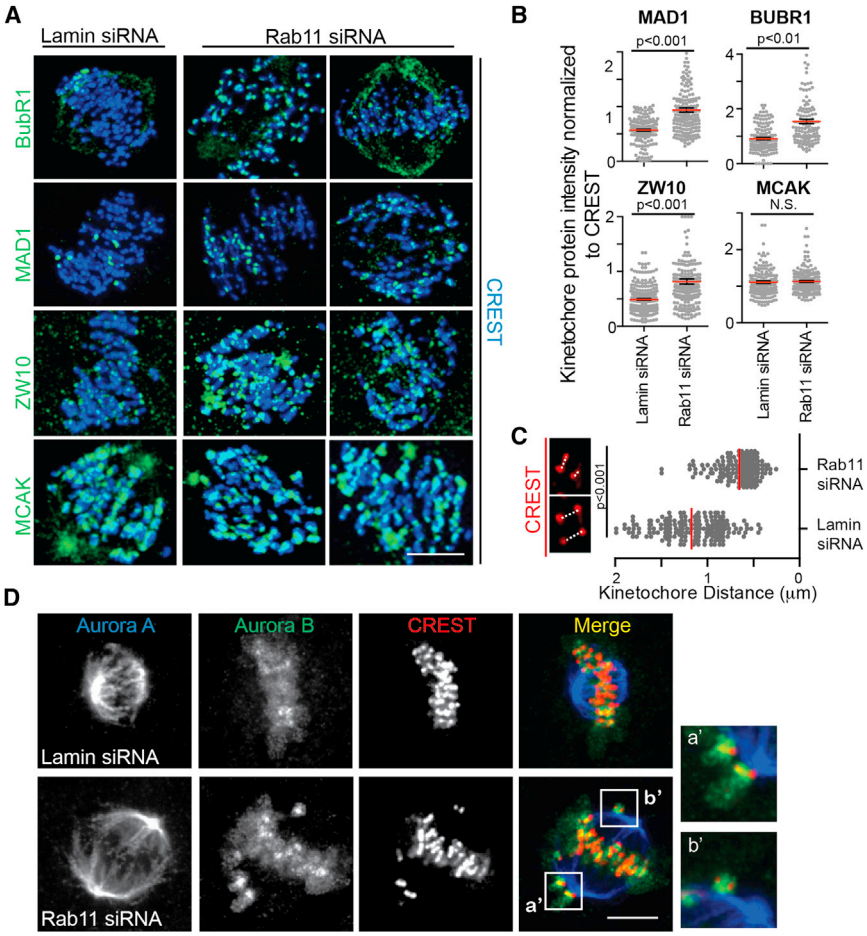


**Figure 7. Rab11 Is Involved in Chromosome Alignment**

(A) The spindle assembly checkpoint proteins BubR1, ZW10, and MAD1 (green) are maintained on kinetochores (CREST, blue) in Rab11-depleted cells compared to control; no difference in MCAK was observed. Scale bar, 5 μm.

(B) Labeled checkpoint proteins were quantified on individual kinetochores and normalized to CREST. A significant increase in MAD1, BUBR1, and ZW10 was observed (n > 200 kinetochores per treatment; p values marked on graph). N.S., nonsignificant. Scale bar, 5 μm.

(C) MT attachments and tension were examined by measuring the distance between two CREST (red) puncta for n > 300 kinetochores, n > 25 cells. Rab11-depleted cells displayed a 2-fold decrease in the distance between kinetochores (~0.5 μm). Refer to p values on graph. Scale bar, 5 μm.

(D) Noncongressed chromosomes in Rab11-depleted cells revealed by staining for Aurora A (blue), Aurora B (green, see insets from boxes), and kinetochores (CREST, red). Representative of n = 10 cells. Scale bar, 5 μm.

See also Figure S6.

diminishes astral MT integrity and inhibits MT attachment to cortical sites essential for orienting spindles. This work reveals a function for Rab11 in spindle pole assembly and spindle orientation. Third, compromised MTs at spindle poles in Rab11-disrupted cells can explain the misaligned chromosomes, mitotic delay, and activation of the SAC. Our results support a pathway for activation of the SAC through poor MT attachments to spindle poles. This pathway is conventionally thought to sense defects in kinetochores-MT attachments, but we contend that poor MT attachments can occur at kinetochores and/or spindle poles (Zimmerman and Doxsey, 2000; Delaval et al., 2011; Firestone et al., 2012). Compromised attachments at either site will prevent MT tension, which is required to satisfy the SAC and permit anaphase onset. The most compelling data for this additional aspect of an old pathway is that kinetochore integrity and function is normal in Rab11 cells (MT nucleation, SAC activation, presence of kinetochore proteins-MCAK, CREST, and p150; data not shown) and is sufficient to drive spindle assembly (at least the early stages) presumably through activation/dominance of the acentrosomal kinetochore/chromatin-based pathway. Within the same Rab11-depleted cells lies the centrosome, which usually acts dominantly in vertebrate cells to drive spindle assembly. However, the deleterious effects of Rab11 depletion compromise the centrosome presumably rendering it inadequate for spindle assembly.

## EXPERIMENTAL PROCEDURES

Reagents and siRNAs are discussed in Supplemental Experimental Procedures.

### Immunofluorescence

A human osteosarcoma cell line, U20S, HeLa-GFP-FIP3 (kind gift from Dr. Rytis Prekeris, University of Colorado), HeLa-GFP-dynein heavy chain (DHC, kind gift from Dr. Cheeseman, MIT), HeLa-GFP-cyclin B/ H2B-RFP (kind gift from Dr. Gerlich), or parental HeLa cells were cultured in D-minimal essential medium (MEM) supplemented with 10% fetal bovine serum (FBS) and 100 U/ml penicillin-streptomycin. HeLa (GFP-FIP3) was kept under selection conditions with Hydromycin B (Sigma). U2OS or HeLa cells were grown to subconfluence on glass coverslips and prepared for immunofluorescence, fixed using either saponin extraction with formaldehyde or methanol (Hehnly et al., 2009). Images were taken on a Perkin-Elmer Ultraview spinning disk confocal microscope: Zeiss Axiovert 200, 100× Plan-APOCROMAT NA1.4 oil, DIC lens, and Hamamatsu ORCA-ER camera. The entire fixed-cell volume was imaged and displayed as a two-dimensional projection (Meta-Morph, Molecular Devices) to ensure that all stained material was visible in two-dimensional images.

### Live-Cell Imaging

Cells were cultured on 35 mm dishes containing a central 14 mm 1.5 glass coverslip (MatTek). Confocal microscopy was performed on a Solamere Technology Group CSU10B Spinning Disk Confocal System attached to a Nikon TE2000-E2 motorized inverted fluorescence microscope. For GFP and RFP, imaging frames were acquired every 100 ms using a Rolera MGi EMCCD 14-bit camera (Qimaging). MetaMorph (Molecular Devices) software was used for equipment control, image acquisition, and image analysis.

### Tracking Vesicle Movement

GFP-FIP3 particles were semiautomatically monitored for 50–100 frames taken every 100 ms in a single z axis using MetaMorph. After configuring MetaMorph to determine intensity centroids for each particle, up to 20 GFP-FIP3 particles paths and velocities were measured per cell. We used 50 μm of ciliobrevin for dynein inhibition (Firestone et al., 2012).

### Transferrin Endocytosis

U2OS or HeLa cells were treated with 10 μg/ml Alexa-Fluor 594-transferrin (Tfn) as described (Hehnly et al., 2012, 2006). The cells were placed at 37°C. The amount of internalized Tfn was detected using fluorescent microscopy.

### Image Analysis

Z stacks are shown as 2D maximum projections (MetaMorph) or processed for 3D rendering (Imaris). Spindle pole fluorescence was quantified as described for the kinetochore, along with kinetochore fluorescence (Howell et al., 2004). Concentric circle regions defined by MetaMorph software (Molecular Devices) were used to define the inner (centrosome or kinetochore) and outer area (local background area was calculated as the difference between the outer and inner circle areas). These circular areas contain the calculated integrated intensities. Cells were counted for three independent experiments as described. Graphs were created and statistical analysis was completed using GraphPad Prism software. Bars represent SE, $p < 0.05$ was considered as statistically significant.

### Membrane Isolation

HeLa GFP-FIP3 cells were washed with a 8% sucrose, 10 mM Tris-HCl, 100 μM GTP, 100 μM ATP, 10 μM BME, and 1 μM PMSF (pH 7.4) buffer, homogenized with a Dounce homogenizer, and spun at 5,000 × *g* for 3 min to generate postnuclear supernatant. The postnuclear supernatant was spun at 50,000 × *g* to generate a membrane pellet, the membrane pellet was then resuspended to a final concentration of 50% sucrose and layered beneath a sucrose step gradient from 40% to 15%. The gradient was placed in the TLA 100.3 rotor and spun at 45,000 × *g* for 2 hr at 4°C (Hehnly et al., 2010). Fractions were collected and run on an SDS-PAGE gel and the fraction containing endosomes saved for in vitro MT regrow experiments.

### In Vitro Microtubule Nucleation from Membranes

The microtubule nucleation solution assays were performed as described with a few modifications (Ori-McKenney et al., 2012; Macurek et al., 2008). GFP-labeled FIP3 endosomes were partially purified from mitotic cells by membrane flotation through a sucrose step gradient, then incubated with 10 μM tubulin/tubulin-Cy3 (cytoskeleton; at a 10:1 ratio) and 1 mM GTP at 37°C for 20 min. The solution was incubated with 4% PFA and spun onto a coverslip. GFP-FIP3-labeled endosomes were counted for Cy3 tubes.

## SUPPLEMENTAL INFORMATION

Supplemental Information includes Supplemental Experimental Procedures, six figures, and four movies and can be found with this article online at http://dx.doi.org/10.1016/j.devcel.2014.01.014.

## ACKNOWLEDGMENTS

This work was supported by National Institutes of Health (NIH) grants GM051994 (to S.D.) and K99GM107355 (to H.H.). We are grateful to Alison Bright, Chun-Ting Chen (Doxsey laboratory), Felix Rivera-Molina, and Derek Toomre (Yale) for their revisions to this manuscript. We thank Mark Stamnes (University of Iowa) for his advice and assistance in the MT membrane in vitro reassembly experiments. We thank Dr. Paul Furcinitti of the Digital Light Microscopy Core Facility at the University of Massachusetts Medical School for assistance with live-cell spinning disk confocal microscopy.

Received: July 29, 2013
Revised: December 4, 2013
Accepted: January 15, 2014
Published: February 20, 2014

## REFERENCES

Ai, E., Poole, D.S., and Skop, A.R. (2009). RACK-1 directs dynactin-dependent RAB-11 endosomal recycling during mitosis in Caenorhabditis elegans. Mol. Biol. Cell *20*, 1629–1638.

Bornens, M. (2012). The centrosome in cells and organisms. Science *335*, 422–426.

Chen, C.-T., Hehnly, H., and Doxsey, S.J. (2012). Orchestrating vesicle transport, ESCRTs and kinase surveillance during abscission. Nat. Rev. Mol. Cell Biol. *13*, 483–488.

Dabbeekeh, J.T.S., Faitar, S.L., Dufresne, C.P., and Cowell, J.K. (2007). The EVI5 TBC domain provides the GTPase-activating protein motif for RAB11. Oncogene *26*, 2804–2808.

Delaval, B., Bright, A., Lawson, N.D., and Doxsey, S. (2011). The cilia protein IFT88 is required for spindle orientation in mitosis. Nat. Cell Biol. *13*, 461–468.

Eldridge, A.G., Loktev, A.V., Hansen, D.V., Verschuren, E.W., Reimann, J.D.R., and Jackson, P.K. (2006). The evi5 oncogene regulates cyclin accumulation by stabilizing the anaphase-promoting complex inhibitor emi1. Cell *124*, 367–380.

Emery, G., Hutterer, A., Berdnik, D., Mayer, B., Wirtz-Peitz, F., Gaitan, M.G., and Knoblich, J.A. (2005). Asymmetric Rab 11 endosomes regulate delta recycling and specify cell fate in the Drosophila nervous system. Cell *122*, 763–773.

Famulski, J.K., and Chan, G.K. (2007). Aurora B kinase-dependent recruitment of hZW10 and hROD to tensionless kinetochores. Curr. Biol. *17*, 2143–2149.

Firestone, A.J., Weinger, J.S., Maldonado, M., Barlan, K., Langston, L.D., O'Donnell, M., Gelfand, V.I., Kapoor, T.M., and Chen, J.K. (2012). Small-molecule inhibitors of the AAA+ ATPase motor cytoplasmic dynein. Nature *484*, 125–129.

Foley, E.A., and Kapoor, T.M. (2013). Microtubule attachment and spindle assembly checkpoint signalling at the kinetochore. Nat. Rev. Mol. Cell Biol. *14*, 25–37.

Heald, R., Tournebize, R., Blank, T., Sandaltzopoulos, R., Becker, P., Hyman, A., and Karsenti, E. (1996). Self-organization of microtubules into bipolar spindles around artificial chromosomes in Xenopus egg extracts. Nature *382*, 420–425.

Hehnly, H., Sheff, D., and Stamnes, M. (2006). Shiga toxin facilitates its retrograde transport by modifying microtubule dynamics. Mol. Biol. Cell *17*, 4379–4389.

Hehnly, H., Longhini, K.M., Chen, J.-L., and Stamnes, M. (2009). Retrograde Shiga toxin trafficking is regulated by ARHGAP21 and Cdc42. Mol. Biol. Cell *20*, 4303–4312.

Hehnly, H., Xu, W., Chen, J.-L., and Stamnes, M. (2010). Cdc42 regulates microtubule-dependent Golgi positioning. Traffic *11*, 1067–1078.

Hehnly, H., Chen, C.-T., Powers, C.M., Liu, H.-L., and Doxsey, S. (2012). The centrosome regulates the Rab11- dependent recycling endosome pathway at appendages of the mother centriole. Curr. Biol. *22*, 1944–1950.

Hobdy-Henderson, K.C., Hales, C.M., Lapierre, L.A., Cheney, R.E., and Goldenring, J.R. (2003). Dynamics of the apical plasma membrane recycling system during cell division. Traffic *4*, 681–693.

Holubcová, Z., Howard, G., and Schuh, M. (2013). Vesicles modulate an actin network for asymmetric spindle positioning. Nat. Cell Biol. *15*, 937–947.

Howell, B.J., Moree, B., Farrar, E.M., Stewart, S., Fang, G., and Salmon, E.D. (2004). Spindle checkpoint protein dynamics at kinetochores in living cells. Curr. Biol. *14*, 953–964.

Kotak, S., and Gönczy, P. (2013). Mechanisms of spindle positioning: cortical force generators in the limelight. Curr. Opin. Cell Biol. *25*, 741–748.

Laflamme, C., Assaker, G., Ramel, D., Dorn, J.F., She, D., Maddox, P.S., and Emery, G. (2012). Evi5 promotes collective cell migration through its Rab-GAP activity. J. Cell Biol. *198*, 57–67.

Lampson, M.A., and Cheeseman, I.M. (2011). Sensing centromere tension: Aurora B and the regulation of kinetochore function. Trends Cell Biol. *21*, 133–140.

Lindqvist, A., Rodríguez-Bravo, V., and Medema, R.H. (2009). The decision to enter mitosis: feedback and redundancy in the mitotic entry network. J. Cell Biol. *185*, 193–202.

Macurek, L., Dráberová, E., Richterová, V., Sulimenko, V., Sulimenko, T., Dráberová, L., Marková, V., and Dráber, P. (2008). Regulation of microtubule

nucleation from membranes by complexes of membrane-bound gamma-tubulin with Fyn kinase and phosphoinositide 3-kinase. Biochem. J. *416*, 421–430.

Mahen, R., and Venkitaraman, A.R. (2012). Pattern formation in centrosome assembly. Curr. Opin. Cell Biol. *24*, 14–23.

Meunier, S., and Vernos, I. (2011). K-fibre minus ends are stabilized by a RanGTP-dependent mechanism essential for functional spindle assembly. Nat. Cell Biol. *13*, 1406–1414.

Ori-McKenney, K.M., Jan, L.Y., and Jan, Y.-N. (2012). Golgi outposts shape dendrite morphology by functioning as sites of acentrosomal microtubule nucleation in neurons. Neuron *76*, 921–930.

Takatsu, H., Katoh, Y., Ueda, T., Waguri, S., Murayama, T., Takahashi, S., Shin, H.-W., and Nakayama, K. (2013). Mitosis-coupled, microtubule-dependent clustering of endosomal vesicles around centrosomes. Cell Struct. Funct. *38*, 31–41.

Theurkauf, W.E., and Hawley, R.S. (1992). Meiotic spindle assembly in Drosophila females: behavior of nonexchange chromosomes and the effects of mutations in the nod kinesin-like protein. J. Cell Biol. *116*, 1167–1180.

Tulu, U.S., Rusan, N.M., and Wadsworth, P. (2003). Peripheral, non-centrosome-associated microtubules contribute to spindle formation in centrosome-containing cells. Curr. Biol. *13*, 1894–1899.

Yadav, S., and Linstedt, A.D. (2011). Golgi positioning. Cold Spring Harb. Perspect. Biol. *3*, 3.

Zhang, H., Squirrell, J.M., and White, J.G. (2008). RAB-11 permissively regulates spindle alignment by modulating metaphase microtubule dynamics in Caenorhabditis elegans early embryos. Mol. Biol. Cell *19*, 2553–2565.

Zimmerman, W., and Doxsey, S.J. (2000). Construction of centrosomes and spindle poles by molecular motor-driven assembly of protein particles. Traffic *1*, 927–934.

Current Biology 22, 1944–1950, October 23, 2012 ©2012 Elsevier Ltd All rights reserved http://dx.doi.org/10.1016/j.cub.2012.08.022

Report

# The Centrosome Regulates the Rab11-Dependent Recycling Endosome Pathway at Appendages of the Mother Centriole

Heidi Hehnly,[1] Chun-Ting Chen,[1] Christine M. Powers,[1] Hui-Lin Liu,[1] and Stephen Doxsey[1,*]
[1]Program in Molecular Medicine, University of Massachusetts Medical School, Biotech 2, Suite 206, 373 Plantation Street, Worcester, MA 01605, USA

## Summary

**The recycling endosome localizes to a pericentrosomal region via microtubule-dependent transport. We previously showed that Sec15, an effector of the recycling endosome component, Rab11-GTPase, interacts with the mother centriole appendage protein, centriolin, suggesting an interaction between endosomes and centrosomes [1, 2]. Here we show that the recycling endosome associates with the appendages of the mother (older) centriole. We show that two mother centriole appendage proteins, centriolin and cenexin/ODF2, regulate association of the endosome components Rab11, the Rab11 GTP-activating protein Evi5, and the exocyst at the mother centriole. Development of an in vitro method for reconstituting endosome protein complexes onto isolated membrane-free centrosomes demonstrates that purified GTP-Rab11 but not GDP-Rab11 binds to mother centriole appendages in the absence of membranes. Moreover, centriolin depletion displaces the centrosomal Rab11 GAP, Evi5, and increases mother-centriole-associated Rab11; depletion of Evi5 also increases centrosomal Rab11. This indicates that centriolin localizes Evi5 to centriolar appendages to turn off centrosomal Rab11 activity. Finally, centriolin depletion disrupts recycling endosome organization and function, suggesting a role for mother centriole proteins in the regulation of Rab11 localization and activity at the mother centriole.**

## Results and Discussion

### The Exocyst, Evi5, and Rab11 Localize to Mother Centriole Appendages

One mother centriole protein, centriolin, interacts with the exocyst subunit Sec15 [1], a known effector of the recycling-endosome GTPase, Rab11 [2, 3]. Because centriolin localizes to subdistal appendages of the mother centriole [1, 4], we asked whether recycling endosome components cofractionated with isolated centrosomes (see Supplemental Experimental Procedures available online, [5]). Sucrose fractions prepared for immunoblotting showed that the endosome components Sec15, Rab11, and the Rab11 GTPase Evi5 [6–8] were enriched in fractions defined by the centrosome components γ-tubulin, centriolin, and pericentrin (Figure S1A; [5]). The ability of these endosomal proteins to associate with isolated centrosomes demonstrated that they were bona fide centrosome components.

Centrosome localization of endosome-associated proteins was initially observed in cells (e.g., Sec15, Sec6, Rab11, and the Rab11 GTPase, Evi5, Figure S1D). To more precisely test for mother centriole localization, we examined centrosome fractions from sucrose gradients that were spun onto coverslips and prepared for immunofluorescence. Quantitative analysis showed a significant fraction of Rab11 (90%), Sec15 (90%), Exo84 (50%), and Evi5 (20%) at the mother centriole (Figures 1A and 1B). These results are likely an underrepresentation, because only centrosomes with exclusive localization to the mother centriole were scored. In contrast, neither Rab8, another GTPase with recycling endosome localization [9], nor the Rab11 effector FIP3 [10, 11] showed significant localization to isolated centrosomes (Figure 1B). It is possible that these proteins may associate but are less integral and lost in the purification process.

We examined mother centriole appendages role in anchoring endosome-associated components. Cenexin/Odf2 is a mother centriole appendage protein whose depletion specifically disrupts the integrity of appendages, but does not affect overall centrosome structure ([12]; Figure 1D; Figures S1C and S1D). Cenexin depletion (Figure 1C) mislocalized the appendage protein centriolin ([12, 13]; Figure 1D), as well as Rab11, Evi5, and the exocyst components Sec15 and Sec6 (Figure 1D; quantification in Figures S1B and S1C). This phenotype was observed in both isolated centrosomes (Figure 1D) and centrosomes in situ (Figure S1D). In parallel studies, centriolin depletion [1] did not affect cenexin localization (Figure S1C). We conclude that several endosome-associated components (Rab11, Evi5, and the exocyst subunits Sec15 and Sec6) require appendages for their localization to the mother centriole.

### Centriolin Regulates Exocyst and Evi5 Mother Centriole Localization

To understand the molecular organization of endosome components at mother centriole appendages, we tested centriole-appendage localization following depletion of appendage or endosome proteins. Centriolin depletion diminished the centrosome localization of the exocyst subunits Sec15, Sec6, and Exo84, as well as Evi5 (Figure 2A). In contrast, depletion of Evi5 (Figure 2A; Figure S2C), Rab11 (Figure 2A; Figure S2A), or Sec15 (data not shown) had no effect on centrosome localization of centriolin, confirming centriolin-anchoring of these molecules (Figure 2A).

We next tested the requirement of centriolin for Sec15 mother centrosome localization using a competition assay (Figure 2B; Figure S2B). When expressed in cells, the centriolin Nud1 domain, previously shown to interact with Sec15 [1], decreased mother-centriole-associated Sec15 in isolated centrosome preparations (2-fold, Figure 2B). In contrast, the centriolin C terminus, which does not interact with Sec15 [1], had no significant effect. Taken together, these findings suggest a hierarchy of centrosome organization, where cenexin and appendages anchor centriolin, which, in turn, anchors Sec15 and Evi5 (Figure 2A).

We confirmed that myc-tagged-Evi5 coimmunoprecipitated Rab11 [7, 8], as well as the exocyst subunit, Exo84 and centriolin (Figure S2D). Thus, the molecular organization of this subcomplex at the centrosome was examined. Sec6 depletion

*Correspondence: stephen.doxsey@umassmed.edu

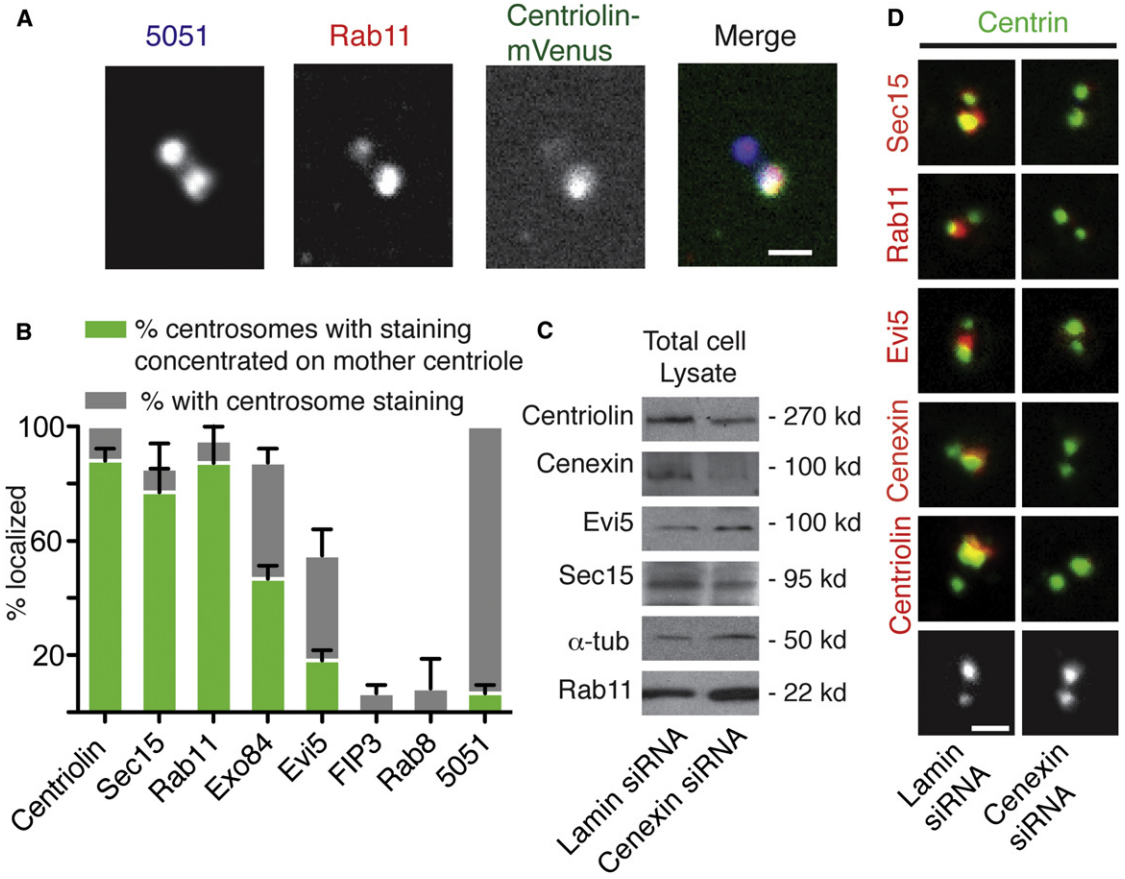


Figure 1. Recycling Endosome Components Associate with Appendages of the Mother Centriole

(A) Membrane-free centrosomes were isolated from cells expressing centriolin-mVenus (green), spun onto glass coverslips [31] and stained for centrosomes (5051, blue) and Rab11 (red). Rab11 costained with centriolin-mVenus, which was concentrated on the mother centriole [4]. Merge of 5051, centriolin-mVenus, and Rab11 signals are shown in white. Scale bar represents 1 μm.

(B) Percentage of Sec15, Rab11, Exo84, Evi5, FIP3, Rab8, centriolin, and 5051 that localize to isolated centrosomes (both centrioles) and concentrate on the mother centriole (as in A), (n = 3 independent experiments; error bar is SE, 150 centrosomes/bar).

(C) Cell lysates from cells treated with lamin (control) or cenexin siRNAs show cenexin depletion and no significant changes in the levels of other proteins.

(D) Isolated centrosomes (as in A) from cells depleted of cenexin or lamin were stained for centrin (green), Sec15 (red), Rab11 (red), Evi5 (red), centriolin (red), and cenexin (red). Bottom images show centrin.

caused the expected decrease in centrosome-associated Sec6 and Sec15, suggesting exocyst complex disruption (Figure 2C). Moreover, exocyst disruption mislocalized Evi5 from centrosomes (Figure 2C). In contrast, Evi5 depletion had no effect on centrosome association of the exocyst (Figure 2A) suggesting that the centriolin-bound-exocyst anchors Evi5 at centrosomes (Figure 2D). We conclude that centriolar-appendage-bound centriolin anchors the exocyst and Evi5.

### Rab11 Activity Governs Its Association with Mother Centriole Appendages

The dependency of Rab11 on cenexin (Figure 1D) for its localization to the mother centriole, suggested that these proteins might interact. This idea was supported by related data showing that a cenexin splice variant, cenexin-3, which localizes to the primary cilium, interacts with Rab8-GTP [14]. Rab8 and Rab11 share certain effectors that include the exocyst subunit Sec15 [2], and they may share others. Immunoprecipitated Rab11 pulled down full-length endogenous cenexin. In a reciprocal experiment, cenexin immunoprecipitation pulled down Rab11 (Figure S3A). In addition, full-length cenexin expressed in cells and a C-terminal cenexin domain (GFP-T6) interacted with Rab11 but an N-terminal domain did not (GFP-T3) (Figure S3B). To our knowledge, this is the first demonstration of an interaction between the endosome protein Rab11 and the centrosome appendage protein cenexin. This interaction may provide the structural and functional link between the endosome and centrosome.

We tested whether the GTP-binding state of Rab11 plays a role in its ability to associate with cenexin (Figure S3C) and more importantly, the mother centriole (Figure 3A; Figure S3D). Cenexin showed a significant preference for the constitutively-active Rab11 (Q70L) compared to the dominant-negative form (Rab11-S25N) (Figure S3D). Immunofluorescence staining of isolated centrosomes from cells expressing Rab11 (Q70L) and wild-type (WT) Rab11 showed colocalization with the mother centriole ~80% of the time, compared with ~20% for the dominant-negative Rab11 (S25N, Figure S3D).

Based on these findings, we developed an in vitro assay for reconstituting endosome protein complexes on isolated centrosomes to test for direct binding of purified bacterially expressed GST-Rab11 to centrosomes in the absence of microtubules and membranes. We found that GST-Rab11 coupled to the GTP analog, GTPγS, showed increased binding

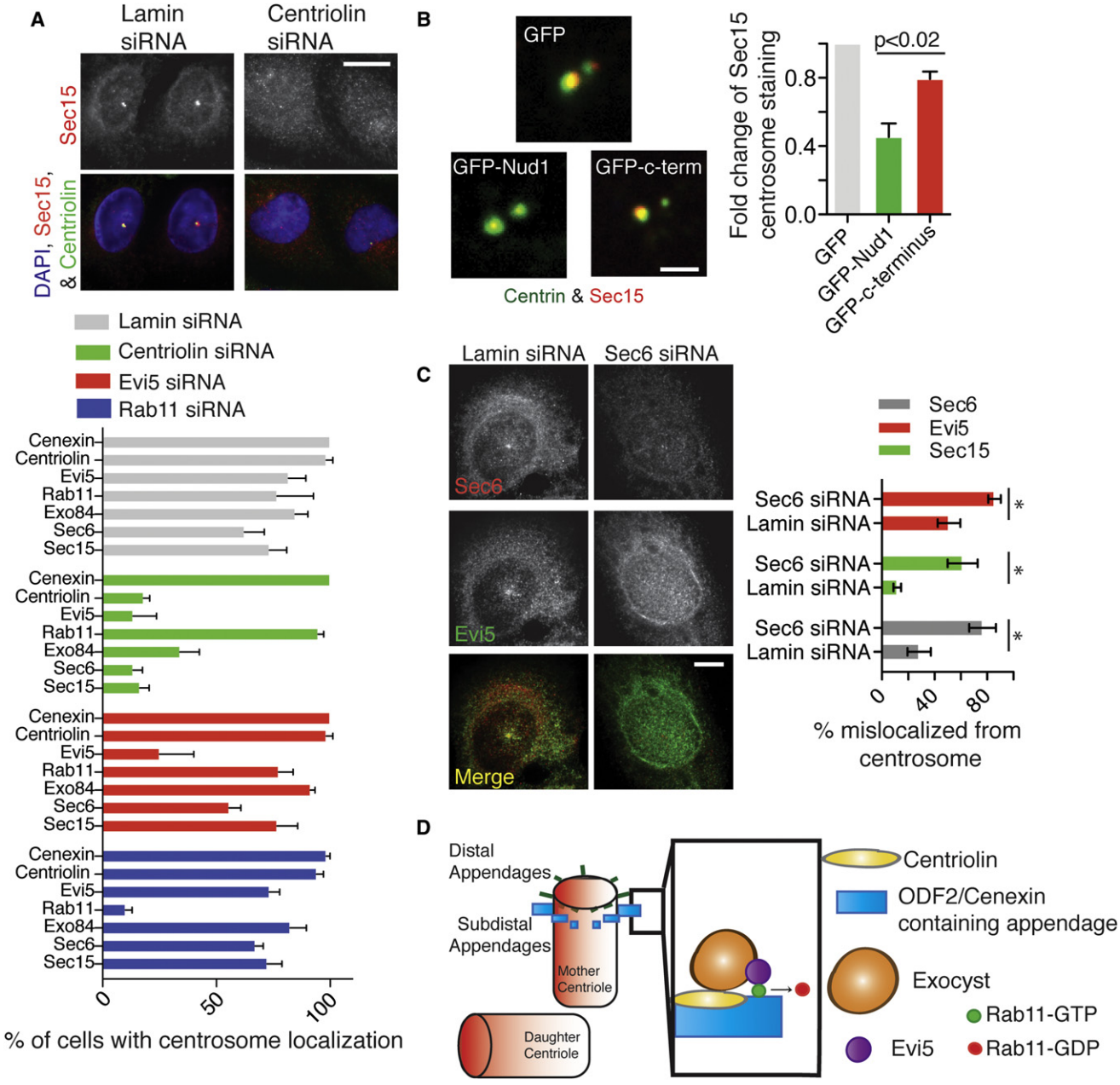


Figure 2. Centriolin Regulates the Centrosomal Localization of the Exocyst and Evi5

(A) Cells stably expressing centriolin-mVenus (green) were stained for Sec15 (red). Scale bar represents 10 μm. Below the immunofluorescence images, we show the percent of cells with centrosome (stained with 5051) localized Sec15, Sec6, Exo84, Rab11, Evi5, centriolin, or cenexin. These values were calculated in cells treated with siRNAs targeting lamin, Rab11, centriolin, or Evi5 (n = 3 experiments, n = 50 centrosomes/treatment/experiment. Error bar is SE).
(B) Centrosomes isolated from cells expressing GFP, GFP-Nud1, or GFP-C terminus were stained for centrin (green) and Sec15 (red). On the right, the fold-change of Sec15 on isolated centrosomes was calculated (n = 3 experiments, $p < 0.02$, n > 25 centrosomes/treatment. Error bar is SE).
(C) Left, exocyst disruption (Sec6 depletion) diminishes Evi5 and Sec15 signal at centrosome. On the right, the quantification of percent of cells with no centrosome localization is shown (n = 3 experiments, *p values < 0.02, error bar is SE). Lamin depletion was used as control.
(D) Proposed structural model for the hierarchy of molecular anchoring at the mother centriole: (1) cenexin anchors centriolin at the appendages of the mother centriole, (2) centriolin anchors its binding partner the exocyst, and (3) the exocyst anchors Evi5, which is a known binding partner of Rab11-GTP and its proposed GAP.

to the mother centriole compared to GST-Rab11 coupled to GDP (2.5-fold, Figure 3A). Importantly, binding of GST-Rab11-GTPγS to isolated centrosomes was inhibited in cells depleted of cenexin (Figure 3A). These biochemical and morphological data show that GTP-bound Rab11 preferentially associates with the mother centriole, through cenexin.

To assess the role of Rab11 activity in mother centriole association, a centrosome-localized Rab11 GAP, we depleted Evi5 [6–8], from cells ([15]; Figure S2C). Evi5 depletion significantly increased Rab11 (Rab11-GTP) at the mother centriole (Figure S3E). We showed that this was due to Evi5 GAP activity by comparing the amount of active-Rab11 in Evi5

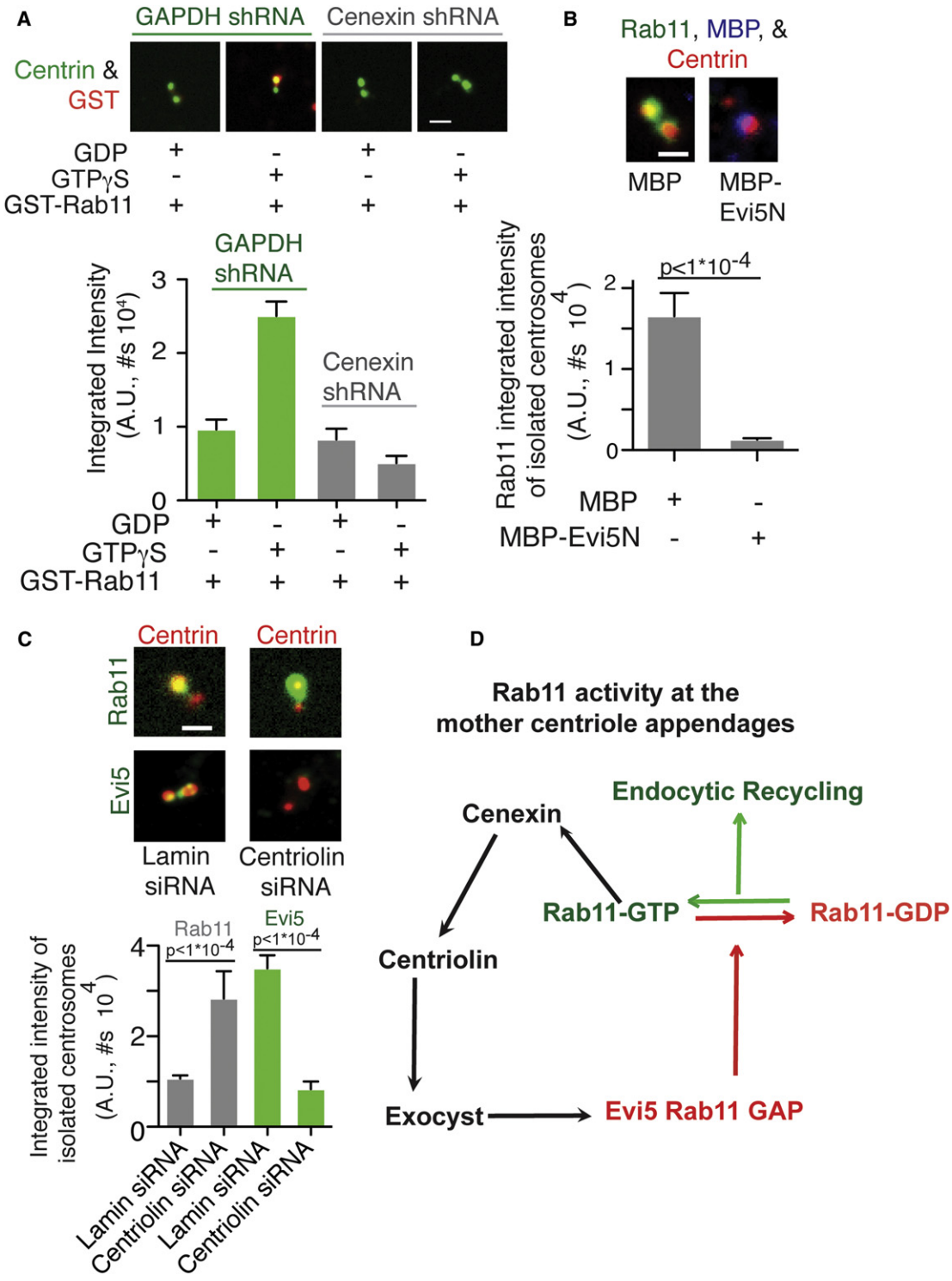


Figure 3. Membrane-free Rab11-GTP Specifically Associates with Cenexin at Mother Centrioles

(A) Isolated centrosomes from GAPDH- or cenexin-depleted cells were incubated with purified GST-Rab11-GTPγS or GST-Rab11-GDP, spun onto glass coverslips, and stained for centrin (green) and GST (red). Below, GST intensity at centrosome was calculated. Representative of n = 3 experiments, n > 100 centrosomes per condition. P value is $p < 1 \times 10^{-4}$ between Rab11-GDP and Rab11- GTPγS in control cells; error bar is SE.

(B) Isolated centrosomes were incubated with purified MBP or MBP-Evi5N, spun onto glass coverslips, stained for Rab11 (green), MBP (blue), or centrin. Below, Rab11 intensity at centrosome was calculated. Representative of n = 3 experiments, n > 30 centrosomes/condition. P value is $p < 1 \times 10^{-4}$. Error bar is SE.

(C) Isolated centrosomes from cells depleted of centriolin were stained for centrin (red), Evi5 (green), and Rab11 (green). Scale bar represents 1 μm. Below, Rab11 (gray) or Evi5 (green) intensity at the centrosome was calculated. Representative of n = 3 experiments with p value $< 1 \times 10^{-4}$, n > 50 centrosomes/treatment/experiment; error bar is SE.

(D) Model for regulating Rab11 activity at the mother centriole. Cenexin organizes centriolin, Exocyst, and Evi5. The mother centriole localization of Evi5 can then act on Rab11-GTP and convert it to inactive Rab11-GDP.

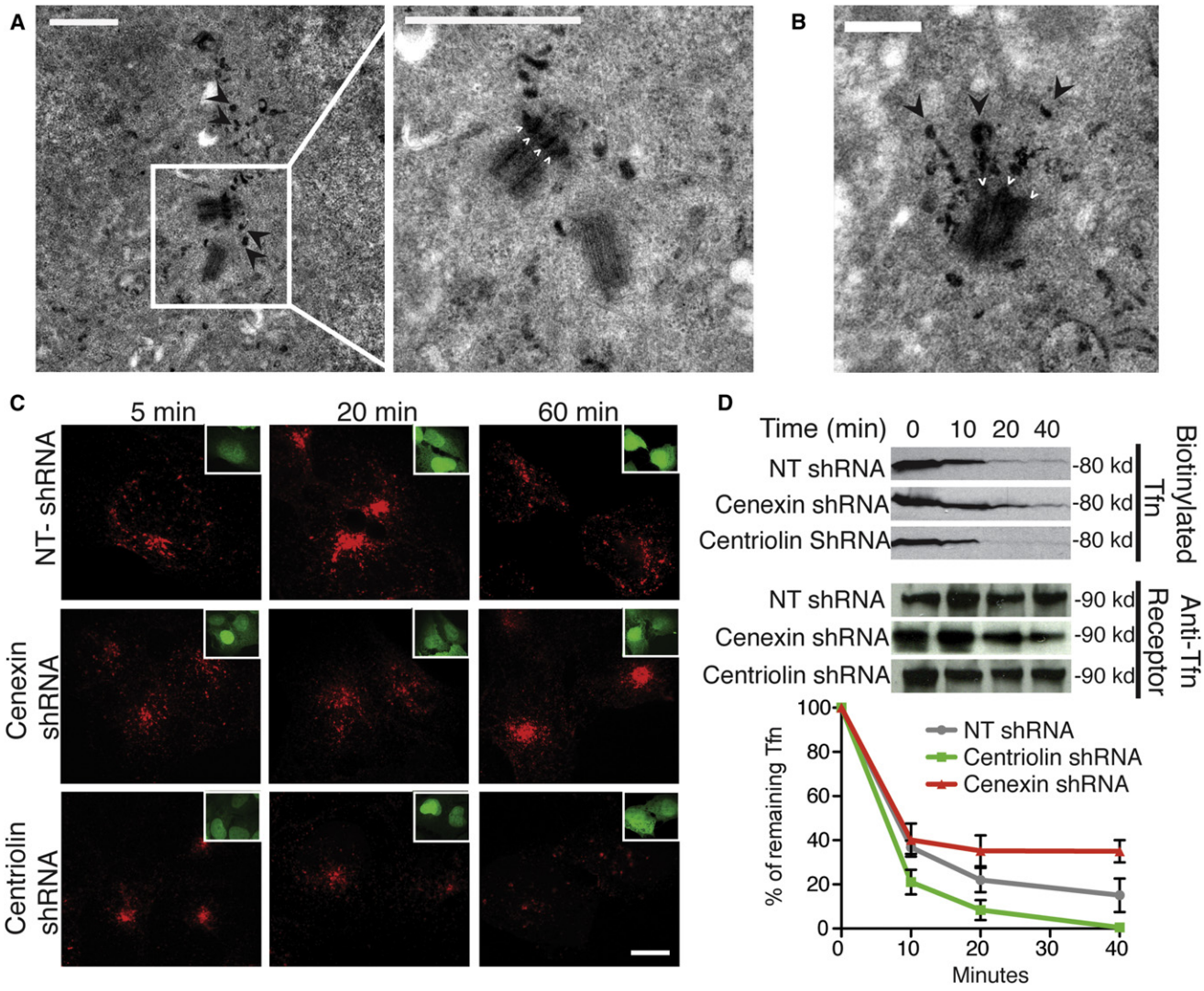


Figure 4. Mother Centriole Appendage Protein Depletion Disrupts Recycling Endosome Function

(A) TEM of cells after endocytosis of Tfn-HRP-DAB, showing reaction product around the mother centriole and concentrated near appendages (four small white arrows, right panel). Arrowheads (black) depict "trails" of Tfn in left and right panels. Scale bar represents 1 μm.

(B) Image of a single centriole with electron-dense Tfn-HRP-DAB filled endosomes emanating from what appear to be centriole appendages (small white arrows indicate appendages; large black arrowheads indicate "endosome trails" of Tfn). Scale bar represents 500 nm.

(C and D) Cells were treated with centriolin small hairpin RNA (shRNA), nontargeting (NT) shRNA (control), or cenexin shRNA.

(C) Cells were incubated with Alexa Fluor 594-conjugated Tfn (red) and chased for up to 60 min with nonconjugated Tfn. Cells were fixed at the indicated times. Insets show cells with GFP-shRNA expression.

(D) Biotinylated-Tfn filled cells were chased with nonconjugated Tfn for indicated times. Biotinylated-Tfn levels were quantified by densitometry (the difference between NT-shRNA and centriolin shRNA or cenexin shRNA at 40 min is statistically significant, p value < 0.05, n = 3 experiments, error bar is SE).

depleted cells compared to control (Figure S4D). In a reciprocal experiment, a maltose-binding protein (MBP)-tagged bacterially expressed Evi5 N-terminal GAP domain (MBP-Evi5N) ([16, 17]; Figure 3B) was purified and added to isolated centrosomes. This induced a decrease in endogenous mother-centriole-associated Rab11 (versus, MBP alone, Figure 3B). Taken together, the increase in active Rab11 at the mother centriole (1) in the in vitro Rab11 centrosome binding experiments (Figure 3A), (2) in cells depleted of Evi5 (Figure S3E), and (3) in cells expressing Rab11 mutants (Figure S3D) provides strong evidence for a model in which the association of Rab11 with the mother centriole appendages is specific and enhanced when the GTPase is in its active, GTP-bound state.

We examined the relationship between Rab11 and Evi5. Earlier, we showed that Evi5 is mislocalized from mother centriole appendages upon cenexin or centriolin depletion (Figures 1D and 2A). In contrast, Rab11 is mislocalized from appendages only in cenexin-depleted cells (Figures 1D and 2A). When isolated centrosomes were prepared from centriolin-depleted cells lacking Evi5 (Figure 3C), there was a significant mother-centriole-specific increase in Rab11 levels (Figure 3C). We propose a model where Evi5 bound to cenexin through centriolin regulates the activity of cenexin-bound

Rab11 at the mother centriole and possibly endocytic recycling (Figure 3D).

### Endosomes Are Organized around Mother Centriole Appendages, and Their Recycling Activity Requires Centrosome-Associated Endosome Proteins

We have shown that endosome proteins localize to mother centriole appendages. We next asked whether centrosome-anchored endosome components regulate endosome organization and function. We examined endosome organization at the centrosome by labeling endosomal compartments with transferrin (Tfn)-HRP (horseradish peroxidase) (see Supplemental Experimental Procedures) and examined the electron-dense Tfn-HRP reaction product by transmission electron microscopy (TEM). We found that endosomes were primarily localized to one centriole (Figure 4A). Moreover, most were organized into multiple discrete elongated periodic structures around the distal aspect of one centriole, ultrastructural features highly reminiscent of subdistal appendages (Figure 4A, white arrows) [4, 18, 19]. In fact, the majority of microtubules emanating from this centriole was consistent with the unique microtubule anchoring function of mother centriole subdistal appendages (Figure 4A) [19, 20]. Other Tfn-labeled compartments were organized into linear assemblies of vesicles and tubules in the pericentrosomal area (Figures 4A and 4B, black arrowheads), suggestive of vectorial transport of endosomes to and from the mother centriole.

To test the role of centrosome-anchored endosome components in endosome recycling, we first examined Tfn-recycling in a pulse-chase experiment ([21]; Figures 4C and 4D). Depletion of centriolin had no detectable effect on microtubule organization or centrosome integrity (Figure S4A; [4]) but increased the rate of Tfn recycling (Figures 4C and 4D). Initially, there was no observable difference in the amount of Tfn in cells (0 to 10 min), but from 20 to 40 min, centriolin-depleted cells contained less Tfn (Figure 4D). In contrast, cenexin depletion decreased Tfn recycling and caused Tfn to accumulate in a juxtacentrosome recycling endosome.

Inspection of centriolin-depleted cells revealed an increase in Rab11 immunofluorescence intensity at centrosomes compared with controls (Figure S4B). There were no gross defects in early endosome (Figure S4A) or transferrin receptor organization (Figure S4A), suggesting that centriolin depletion selectively disrupted Rab11 localization in cells. To test for Rab11 activity changes, we used two approaches. We isolated a membrane fraction as a read-out of GTP-bound Rab11 [22]. We also immunoprecipitated active-Rab11 using a cell line expressing its effector GFP-FIP3 [10]. In both cases, centriolin depletion increased Rab11 (~2-fold, Figures S4C and S4D), consistent with an increased amount of active-GTP-bound Rab11.

We propose that centriolin-depleted cells lose Evi5, causing active Rab11 to be retained on centrosomes (Figure 3C) causing an increase in centrosome-bound Rab11-GTP (Figure 3C; Figure S4B). We suggest that the enhanced recycling (Figure 4D) is due to an increase in the ability of the centrosome-bound fraction of Rab11 to recycle cargo from the recycling endosome to the plasma membrane at a faster rate. In contrast, cenexin depletion inhibits the ability of Rab11 to recycle endosomes (Figure 4D) due to loss of appendage-bound Rab11 (Figure 1D). These findings support and add to our in vitro binding studies (Figure 3A) by illustrating that the association of Rab11 with the mother centriole is important for efficient recycling through the juxtacentrosomal recycling endosome.

In conclusion, it has been known for some time that recycling endosomes are found in the pericentrosomal area and are influenced by Rab11 activity. However, little is known about the relationship between these juxtaposed organelles at the structural, molecular, or functional level. Here we show that the appendages of the mother centriole and recycling endosomes are in intimate contact (Figures 4A and 4B). We show that Rab11 and its GAP, Evi5, are linked to the centriolar appendages through the centrosome proteins cenexin and centriolin (Figures 1 and 2). This is the first evidence for a novel centrosome-anchored molecular pathway for the inactivation of Rab11 and regulation of endosome recycling through a complex series of protein interactions and activities.

The discovery of a structural association between the endosome and the centrosome with complex molecular underpinnings has new and unexpected implications for recycling endosome function. This new liaison has additional implications for a variety of biological processes including cilia formation and function [9, 23], asymmetric cell division [24–27], and cell polarity [28, 29]. It is also likely that centrosome function will itself be influenced through its association with the endosome, although this has yet to be explored. The latter brings up an intriguing question: Do recycling endosomes bound to centrosomes impart properties to centrosome activities, known and new? One result that suggests this might be the case is the dual role of dynamin-2 in both vesicle formation and centrosome cohesion [30]. Thus, it is also possible that Rab11 and other endosome-associated molecules bound to the centrosome may play dual roles in endosome and centrosome function. This observation and the endosome-centrosome connection, lead us to speculate that the centrosome may directly associate with other (membranous) organelles, such as the Golgi apparatus or endoplasmic reticulum, generating a new repertoire of previously unappreciated combined functions for both organelles. Future investigations will be required to test these ideas.

#### Supplemental Information

Supplemental Information includes four figures and Supplemental Experimental Procedures and can be found with this article online at http://dx.doi.org/10.1016/j.cub.2012.08.022.

#### Acknowledgments

We thank Mary Munson and David Lambright (UMMS), Alison Bright and Tse-Chun Kuo (UMMS, Doxsey Lab), and Charles Yeaman (University of Iowa) for reading versions of this manuscript. The following grants supported this work S10RR027897 (TEM, UMMS), 2R01 GM051994-15A2 (S.D.), and F32 GM095161-01 (H.H.).

Received: March 13, 2012
Revised: July 16, 2012
Accepted: August 13, 2012
Published online: September 13, 2012

#### References

1. Gromley, A., Yeaman, C., Rosa, J., Redick, S., Chen, C.T., Mirabelle, S., Guha, M., Sillibourne, J., and Doxsey, S.J. (2005). Centriolin anchoring of exocyst and SNARE complexes at the midbody is required for secretory-vesicle-mediated abscission. Cell *123*, 75–87.
2. Wu, S., Mehta, S.Q., Pichaud, F., Bellen, H.J., and Quiocho, F.A. (2005). Sec15 interacts with Rab11 via a novel domain and affects Rab11 localization in vivo. Nat. Struct. Mol. Biol. *12*, 879–885.
3. Zhang, X.-M., Ellis, S., Sriratana, A., Mitchell, C.A., and Rowe, T. (2004). Sec15 is an effector for the Rab11 GTPase in mammalian cells. J. Biol. Chem. *279*, 43027–43034.

4. Gromley, A., Jurczyk, A., Sillibourne, J., Halilovic, E., Mogensen, M., Groisman, I., Blomberg, M., and Doxsey, S. (2003). A novel human protein of the maternal centriole is required for the final stages of cytokinesis and entry into S phase. J. Cell Biol. *161*, 535–545.
5. Mitchison, T., and Kirschner, M. (1984). Microtubule assembly nucleated by isolated centrosomes. Nature *312*, 232–237.
6. Faitar, S.L., Dabbeekeh, J.T.S., Ranalli, T.A., and Cowell, J.K. (2005). EVI5 is a novel centrosomal protein that binds to alpha- and gamma-tubulin. Genomics *86*, 594–605.
7. Dabbeekeh, J.T.S., Faitar, S.L., Dufresne, C.P., and Cowell, J.K. (2007). The EVI5 TBC domain provides the GTPase-activating protein motif for RAB11. Oncogene *26*, 2804–2808.
8. Laflamme, C., Assaker, G., Ramel, D., Dorn, J.F., She, D., Maddox, P.S., and Emery, G. (2012). Evi5 promotes collective cell migration through its Rab-GAP activity. J. Cell Biol. *198*, 57–67.
9. Knödler, A., Feng, S., Zhang, J., Zhang, X., Das, A., Peränen, J., and Guo, W. (2010). Coordination of Rab8 and Rab11 in primary ciliogenesis. Proc. Natl. Acad. Sci. USA *107*, 6346–6351.
10. Wilson, G.M., Fielding, A.B., Simon, G.C., Yu, X., Andrews, P.D., Hames, R.S., Frey, A.M., Peden, A.A., Gould, G.W., and Prekeris, R. (2005). The FIP3-Rab11 protein complex regulates recycling endosome targeting to the cleavage furrow during late cytokinesis. Mol. Biol. Cell *16*, 849–860.
11. Fielding, A.B., Schonteich, E., Matheson, J., Wilson, G., Yu, X., Hickson, G.R., Srivastava, S., Baldwin, S.A., Prekeris, R., and Gould, G.W. (2005). Rab11-FIP3 and FIP4 interact with Arf6 and the exocyst to control membrane traffic in cytokinesis. EMBO J. *24*, 3389–3399.
12. Ishikawa, H., Kubo, A., Tsukita, S., and Tsukita, S. (2005). Odf2-deficient mother centrioles lack distal/subdistal appendages and the ability to generate primary cilia. Nat. Cell Biol. *7*, 517–524.
13. Soung, N.-K., Park, J.E., Yu, L.R., Lee, K.H., Lee, J.M., Bang, J.K., Veenstra, T.D., Rhee, K., and Lee, K.S. (2009). Plk1-dependent and -independent roles of an ODF2 splice variant, hCenexin1, at the centrosome of somatic cells. Dev. Cell *16*, 539–550.
14. Yoshimura, S.-I., Egerer, J., Fuchs, E., Haas, A.K., and Barr, F.A. (2007). Functional dissection of Rab GTPases involved in primary cilium formation. J. Cell Biol. *178*, 363–369.
15. Faitar, S.L., Sossey-Alaoui, K., Ranalli, T.A., and Cowell, J.K. (2006). EVI5 protein associates with the INCENP-aurora B kinase-survivin chromosomal passenger complex and is involved in the completion of cytokinesis. Exp. Cell Res. *312*, 2325–2335.
16. Eldridge, A.G., Loktev, A.V., Hansen, D.V., Verschuren, E.W., Reimann, J.D., and Jackson, P.K. (2006). The evi5 oncogene regulates cyclin accumulation by stabilizing the anaphase-promoting complex inhibitor emi1. Cell *124*, 367–380.
17. Westlake, C.J., Junutula, J.R., Simon, G.C., Pilli, M., Prekeris, R., Scheller, R.H., Jackson, P.K., and Eldridge, A.G. (2007). Identification of Rab11 as a small GTPase binding protein for the Evi5 oncogene. Proc. Natl. Acad. Sci. USA *104*, 1236–1241.
18. Doxsey, S.J., Stein, P., Evans, L., Calarco, P.D., and Kirschner, M. (1994). Pericentrin, a highly conserved centrosome protein involved in microtubule organization. Cell *76*, 639–650.
19. Bornens, M. (2012). The centrosome in cells and organisms. Science *335*, 422–426.
20. Delgehyr, N., Sillibourne, J., and Bornens, M. (2005). Microtubule nucleation and anchoring at the centrosome are independent processes linked by ninein function. J. Cell Sci. *118*, 1565–1575.
21. Sheff, D.R., Daro, E.A., Hull, M., and Mellman, I. (1999). The receptor recycling pathway contains two distinct populations of early endosomes with different sorting functions. J. Cell Biol. *145*, 123–139.
22. Zerial, M., and McBride, H. (2001). Rab proteins as membrane organizers. Nat. Rev. Mol. Cell Biol. *2*, 107–117.
23. Westlake, C.J., Baye, L.M., Nachury, M.V., Wright, K.J., Ervin, K.E., Phu, L., Chalouni, C., Beck, J.S., Kirkpatrick, D.S., Slusarski, D.C., et al. (2011). Primary cilia membrane assembly is initiated by Rab11 and transport protein particle II (TRAPPII) complex-dependent trafficking of Rabin8 to the centrosome. Proc. Natl. Acad. Sci. USA *108*, 2759–2764.
24. Emery, G., Hutterer, A., Berdnik, D., Mayer, B., Wirtz-Peitz, F., Gaitan, M.G., and Knoblich, J.A. (2005). Asymmetric Rab 11 endosomes regulate delta recycling and specify cell fate in the Drosophila nervous system. Cell *122*, 763–773.
25. Januschke, J., Llamazares, S., Reina, J., and Gonzalez, C. (2011). Drosophila neuroblasts retain the daughter centrosome. Nature communications *2*, 243.
26. Wang, X., Tsai, J.W., Imai, J.H., Lian, W.N., Vallee, R.B., and Shi, S.H. (2009). Asymmetric centrosome inheritance maintains neural progenitors in the neocortex. Nature *461*, 947–955.
27. Yamashita, Y.M., Mahowald, A.P., Perlin, J.R., and Fuller, M.T. (2007). Asymmetric inheritance of mother versus daughter centrosome in stem cell division. Science *315*, 518–521.
28. Feldman, J.L., and Priess, J.R. (2012). A Role for the Centrosome and PAR-3 in the Hand-Off of MTOC Function during Epithelial Polarization. Curr Biol *22*, 575–582.
29. Hehnly, H., and Doxsey, S. (2012). Polarity sets the stage for cytokinesis. Mol. Biol. Cell *23*, 7–11.
30. Thompson, H.M., Cao, H., Chen, J., Euteneuer, U., and McNiven, M.A. (2004). Dynamin 2 binds gamma-tubulin and participates in centrosome cohesion. Nat. Cell Biol. *6*, 335–342.
31. Blomberg-Wirschell, M., and Doxsey, S.J. (1998). Rapid isolation of centrosomes. Methods Enzymol. *298*, 228–238.

Review

# Resurrecting remnants: the lives of post-mitotic midbodies

Chun-Ting Chen[1,*], Andreas W. Ettinger[2,*], Wieland B. Huttner[3], and Stephen J. Doxsey[1]

[1] Program in Molecular Medicine, University of Massachusetts Medical School, Worcester, MA 01605, USA
[2] Department of Cell & Tissue Biology, University of California San Francisco, San Francisco, CA 94143, USA
[3] Max Planck Institute of Molecular Cell Biology and Genetics, Dresden, Germany

**Around a century ago, the midbody (MB) was described as a structural assembly within the intercellular bridge during cytokinesis that served to connect the two future daughter cells. The MB has become the focus of intense investigation through the identification of a growing number of diverse cellular and molecular pathways that localize to the MB and contribute to its cytokinetic functions, ranging from selective vesicle trafficking and regulated microtubule (MT), actin, and endosomal sorting complex required for transport (ESCRT) filament assembly and disassembly to post-translational modification, such as ubiquitination. More recent studies have revealed new and unexpected functions of MBs in post-mitotic cells. In this review, we provide a historical perspective, discuss exciting new roles for MBs beyond their cytokinetic function, and speculate on their potential contributions to pluripotency.**

## An overview of the MB assembly

Cell division requires segregation of the duplicated genome and partitioning of cellular contents between daughter cells during cytokinesis. In animal cells, cytokinesis begins with ingression of the plasma membrane and culminates in a poorly understood event called abscission (see Glossary), where daughter cells become physically separated from one another (for reviews see [1,2]). Recent advances have uncovered several key features of abscission such as membrane trafficking [3] (for reviews, see [4,5]), MT reorganization [6,7], helical filament formation driven by ESCRT [7–9], and regulatory mechanisms involving protein ubiquitination [10,11]. Little is known about how these events are coordinated to achieve abscission other than that they all occur in the vicinity of the MB. Disruption of any of these MB-associated events leads to abscission failure, defining this organelle as a key player in abscission [3,12,13]. One result of abscission failure is polyploidy, a potential factor in cancer predisposition and progression [14] and in multicellular syncytium formation [15].

This review focuses on MB structure and function during cytokinesis and the fate and function of post-mitotic MBs. It has been shown both *in vivo* and *in vitro* that post-mitotic MBs can be released from cells, where they deteriorate with time [16–19]. They can also be retained by cells, where they either degrade or persist for extended periods of time [3,19–23]. Their distinct fates in different cell types can dramatically impact cellular physiology and cell-fate determination [19,22,23]. These new functional roles for post-mitotic MBs have resurrected interest in MB form and function.

## MB characteristics: a historical perspective

### *Biogenesis and architecture of the MB revealed by electron microscopy (EM)*

Walther Flemming first noted the presence of MBs using histochemical methods [24], then others observed MB dynamics by time-lapse light microscopy [25,26] (for details, see Box 1). EM later provided more detail of MBs and associated structures [16,27–33] and again supported the early hypotheses of Flemming (Box 1). EM studies confirmed that the overall structure of the developing MB was strikingly similar to the phragmoplast of plants [34]. Both MB and phragmoplast comprise antiparallel MTs with

### Glossary

**Abscission**: the final stage of cytokinesis that culminates in severing the intercellular bridge to generate two physically separate daughter cells. This process requires several membrane-trafficking pathways, the ESCRT complex, and the machinery for MT severing.
**Autophagosome**: an intracellular double-membrane vacuole/vesicle formed *de novo* that engulfs molecules or organelles from the cytoplasm and degrades them by fusing with lysosomes. Autophagosome formation is known to require the autophagy-related gene (Atg) 6, or Beclin-1, and two ubiquitin-like conjugation systems (e.g., LC3/Atg8).
**Endosomal sorting complex required for transport (ESCRT)**: a protein complex containing four subcomplexes (ESCRT-0, -I, -II, and -III) and associated proteins (e.g., Alix, Ist1, and Vps4) that sorts and transports target molecules to endosomes. It is required for viral budding and has recently been shown to play a role in abscission.
**Exocyst**: a protein complex required for the tethering and targeting of post-Golgi vesicles to the plasma membrane for secretion and abscission.
**Intercellular bridge**: the cytoplasmic connection between a dividing cell in late cytokinesis that contains the MB and is the ultimate site of cell separation.
**Midbody (MB)**: a prominent organelle located within the intercellular bridge. It comprises a central proteinaceous disc or ring-like core flanked by MTs that overlap within the ring region as antiparallel bundles. This core is also referred to as the Flemming body or midbody ring. The MB undergoes many morphological and molecular changes before abscission and is essential for the completion of cell division.
**Multivesicular body (MVB)**: a specialized membranous compartment in the endosomal pathway characterized by internalized vesicles within its lumen. After fusing with lysosomes, the molecular contents within MVBs can be degraded.
**Phragmoplast**: a spindle-derived structure formed during plant cytokinesis. It comprises MTs, actin, and various membranous components and is required for completion of cytokinesis.
**Soluble N-ethylmaleimide-sensitive factor [NSF] attachment protein receptors (SNAREs)**: this is a large protein superfamily whose major function is to facilitate fusion between vesicles and the membrane of target compartments. SNAREs can thus further be divided to vesicle SNAREs (v-SNAREs), such as endobrevin/VAMP8, and target SNAREs (t-SNAREs), such as syntaxin-2.

*Corresponding authors:* Huttner, W.B. (huttner@mpi-cbg.de); Doxsey, S.J. (stephen.doxsey@umassmed.edu).
*Keywords:* cytokinesis; abscission; midbody; asymmetry; stem cells; cell fates.
* These authors contributed equally to this work.

 0962-8924/$ – see front matter  http://dx.doi.org/10.1016/j.tcb.2012.10.012 Trends in Cell Biology, March 2013, Vol. 23, No. 3

**Box 1. The initial characterization of MBs**

*Early glimpses of the MB*

The MB, or Zwischenkörper ('Zwischen' and 'körper' mean 'between' and 'body', respectively; also referred to as the Flemming body), was first described by Walther Flemming in 1891 [24]. Using light microscopy and histochemical stains, he identified a chromophilic structure positioned between dividing daughter cells (see Figure 1a in main text) and speculated that it was derived from the spindle midzone between segregating chromosomes. He also suggested that it might be the animal counterpart of the phragmoplast, a MT-enriched structure involved in plant cytokinesis (for review, see [70]). In the 1960s and 1970s, with the aid of EM, most of Flemming's prescient theories were validated [27–29,71].

*MB dynamics revealed by time-lapse light microscopy*

Microcinematographic light microscopy in the 1970s showed that the classical MB structure appeared within the intercellular bridge after furrow ingression (see Figure 1b, left and middle panels in main text) [25,26]. In human cells, it formed a disc-like structure approximately 1–2 μm in diameter. As cytokinesis proceeded, the diameter of the intercellular bridge narrowed, whereas the MB size remained relatively constant. With time, the plasma membrane of the bridge wrapped tightly around the MB, creating a bulge in the bridge (see Figure 1b, right panel in main text). Despite this, the MB was able to slide within the bridge between the two connected daughter cells. Later, the intercellular bridge showed 'waving activity' that propagated away from both sides of the MB. The activity ceased initially on one side of the bridge. The other side continued this activity then narrowed to a thin thread of cytoplasm and was severed [25,26]. This observation is also consistent with later studies that defined this and other asymmetric events before abscission (see below and [3,7,9,21,40]).

**Box 2. MB and the associated membrane function as a diffusion barrier**

With the ability to perform high-resolution time-lapse imaging and the generation of various fluorescence tags with different properties, researchers have now been able to test whether a diffusion barrier exists at the MB and associated membrane in the intercellular bridge. It appears that this barrier is selective. Inner-leaflet plasma membrane proteins such as Lyn-GFP and transmembrane proteins such as LYFPGT46 were unable to transverse from one daughter cell to the other, as revealed by photorecovery assays. However, an outer-leaflet plasma membrane protein and a cytosolic protein appeared to pass through, as shown by photorecovery of YGP-GI-GPI and cytosolic GFP, and the microinjection of Lucifer Yellow dye [7,36–38]. The selective passing of molecules could be modulated by channels in the MB that interconnect the cytoplasm of the two daughter cells [16,38] or the space between the associated bridge membrane and the MB core. Only when MB structure and 'permeability' are examined more thoroughly in different cell types and at carefully defined times during the process of cytokinesis will the timing and functional significance for the MB as a barrier emerge.

vesicles and amorphous electron-dense material centrally positioned (for review, see [35]). Also among the MTs of the developing MB was a diversity of membranous organelles, such as endoplasmic reticulum cisternae, Golgi complexes, and electron-lucent and -dense vesicles. Double membrane-bound electron-dense bodies associated with multivesicular bodies (MVBs) and reminiscent of autophagosomes were also found at these sites [16,28,30,32]. After furrow ingression, membranous organelles gradually decreased at MT sites and concomitantly appeared at the junctions of the bridge and cell bodies (Figure 1b, middle panel) [16,29,30,32]). MT bundles coalesced and the amorphous electron-dense material reorganized into a continuous plaque-like structure between daughter cells, the Flemming body [16,28,30–32]. The Flemming body was thought to provide a diffusion barrier between daughter cells. However, more recent work suggests that the barrier might be selective (for details, see Box 2 and [36–38]).

By late cytokinesis, the MB is a prominent structure with a central core, flanking MTs and associated organelles, and the surrounding plasma membrane (Figures 1b and 2a). The MB core has two components, the 'MB matrix' and 'MB ridges'. The MB matrix mainly comprises antiparallel MT bundles and interspersed electron-dense material [16,31,33,39]. MB ridges surrounding the matrix account for the bulges within the intercellular bridge (Figure 2a, bottom panel) and primarily comprise electron-dense material, a specialized thickening under the plasma membrane, and a few MTs [16]. MB ridges are likely to correspond to MB rings (MRs), donut-shaped structures revealed in more recent studies by phase contrast and immunofluorescence (IF) microscopy (Figure 2a, middle panel) [3].

During early stages of abscission, the caliber of the bridge narrows and MT bundles within the bridge are reduced by severing and depolymerization [7,16,33,39–41]. At a site adjacent to the MB (termed the 'narrowing segment' [16] or 'constriction zone' [7]), the bridge caliber narrows further and 'ripple contours' appear (Figure 2b, top panels) [7,16]. Such ripples represent a series of membrane deformations along the bridge membrane, which are the helical filaments built by ESCRT components recently observed at this site (Figure 2b, bottom panel) [7]. In addition to reforming membranous compartments within cell bodies during late cytokinesis, vesicle clusters were frequently observed along MTs in the bridge, concentrated near the MB [16,30,31]. Abscission occurred after vesicles were trafficked to the MB, where they presumably docked and fused [3,21,42], MT bundles were reduced and severed [6,40,41], and ESCRT-containing filaments were organized along the bridge membrane on one or both sides of the MBs [7,9].

### *The fate of post-mitotic MBs*

Early EM studies suggested that post-mitotic MBs were transient structures that were released from cells where they deteriorated [16,28,39], leading to terms such as MB remnant and residual body. These post-mitotic MBs often retained recognizable MB matrix, ridges, antiparallel MTs, and plasma membrane [16]. However, these features were likely to be lost over time [17,18]. Indeed, with the aid of immuno-EM to detect MB molecules, it was shown that the large and relatively homogeneously sized electron-dense particles in brain ventricles were 'aged' post-mitotic MBs that had lost their typical morphological and biochemical signatures [18].

Closer inspection of changes in post-mitotic MB structure over time was enabled by time-lapse imaging, ordering of temporal events, and biochemical analysis. These approaches showed that post-mitotic MBs associated with one of the two daughter cells after abscission [3,18,19,21,22]. Immediately after abscission on one side of the MB, the thin bridge on the other side of the MB retained its connection to the other daughter cell. This tether was reminiscent of the thin stalk described in studies using microcinematography and EM [16,18,25,26]. The tether can retract, delivering the post-mitotic MB into the cytoplasm of one daughter cell for

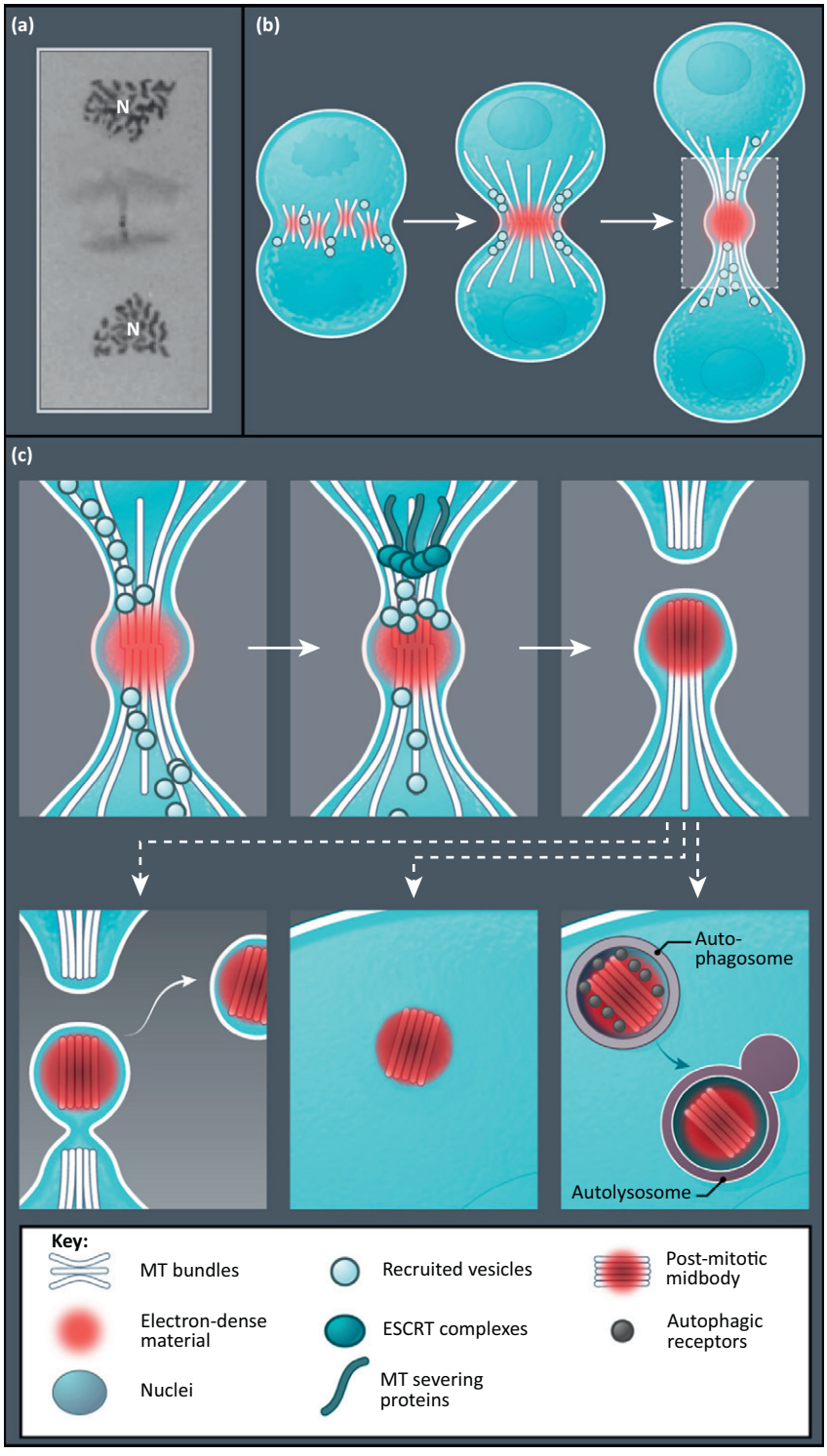


**Figure 1**. Schematic representation of cytokinesis progression, abscission, and the fate of the post-mitotic midbody (MB). (**a**) A representative drawing of Zwischenkörper by Walther Flemming. The black dot between the two reforming nuclei (N) represents the MB (white arrow). **(b)** Progression from early to late cytokinesis is shown from left to right and can be generally dissected into three stages. Left: Antiparallel microtubules (MTs) and electron-dense material initially form a patchwork at the midzone across the forming furrow, where vesicles are concentrated. Middle: After furrow ingression, the patchwork of midzone MTs transforms into one major bundle between two daughter cells and vesicles concentrate at the end of the bundle. Right: As cytokinesis proceeds, the intercellular bridge connecting the two daughter cells is gradually remodeled and narrowed, making the MB a prominent bulge in the bridge. **(c)** Enlargement of inset in (b), showing the process of abscission and the fate of the post-mitotic MB. From left: As the cell approaches the final stage of abscission, the density of MTs decreases and different vesicle types again appear in vicinity of the MB. Meanwhile, endosomal sorting complex required for transport (ESCRT) complexes are recruited to the constriction zone, about 1 μm from the MB, and interact with the MT-severing protein (e.g., spastin). Presumably, abscission requires the orchestration of these pathways (e.g., vesicle trafficking and fusion, ESCRT machinery, and MT severing). After abscission, the post-mitotic MB is either released after a secondary bridge-severing event (bottom left panel) or inherited by one of the two daughter cells (bottom middle and right panels). The inherited MBs may be retained freely in the cytoplasm (bottom middle panel) or degraded in the autolysosome after being recognized by autophagic receptors (grey ovals) and engulfed by autophagosomes (bottom right panel). Thus, two major mechanisms for MB clearance are autophagy and MB release. The drawing of Zwischenkörper was reproduced from [24].

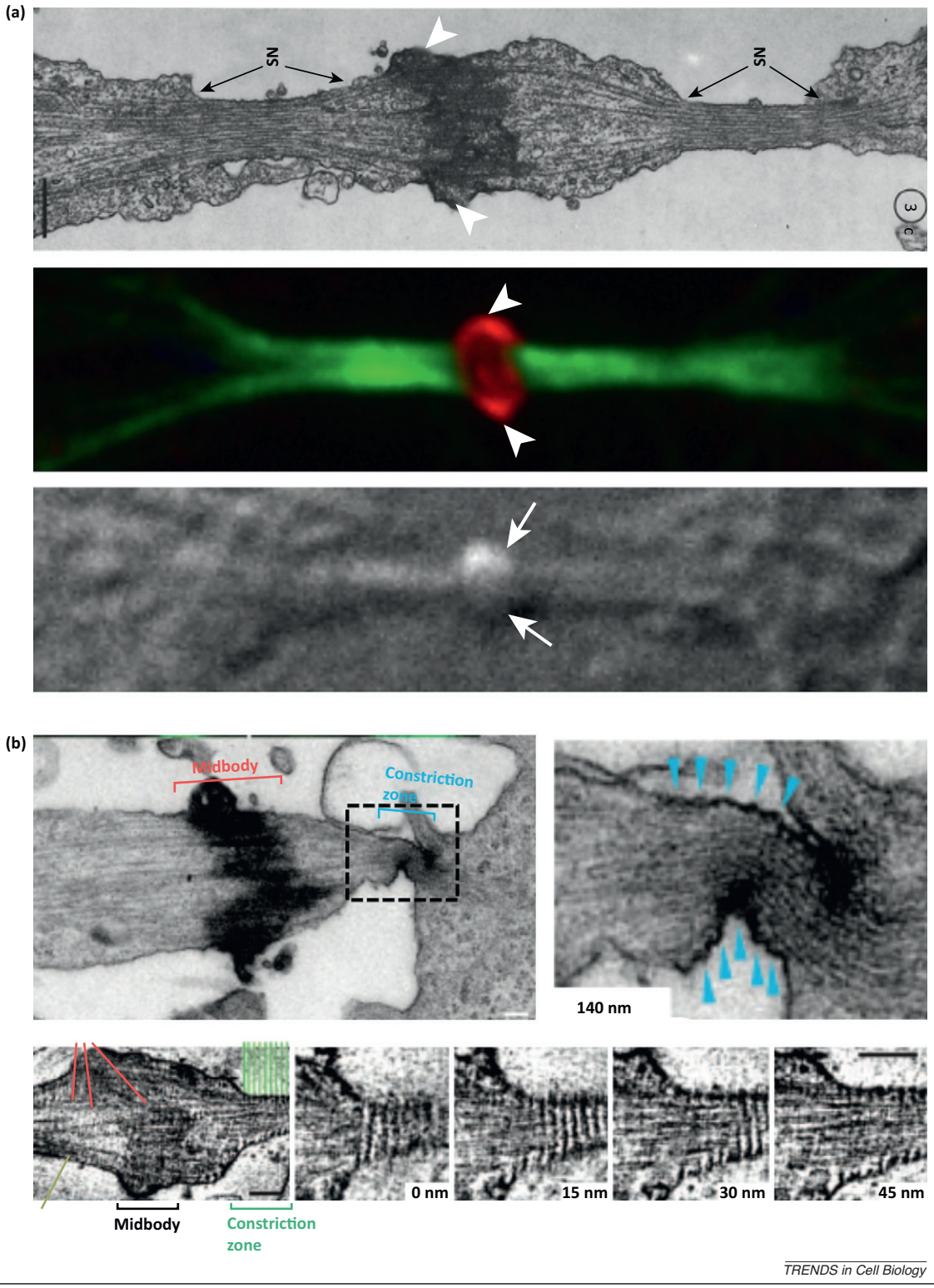


**Figure 2**. The architecture of the midbody (MB) during late cytokinesis and abscission. **(a)** Electron micrograph of a MB is shown in the top panel. An immunostained MB at a comparable stage with corresponding differential-interference contrast (DIC) microscope image are shown in the middle and bottom panel, respectively. At the center is the electron-dense MB core (top), which comprises 'MB ridges' and 'MB matrix'. The MB ridges (arrowheads; top) correspond to the bulge on DIC microscopy (arrows; bottom) and the MB ring (MR) on immunofluorescence (arrowheads; middle). The MB matrix, by contrast, contains many antiparallel microtubules (MTs) and electron-dense material. α-Tubulin, intercellular bridge (green); Mklp1, MB (red). **(b)** Electron micrograph of a MB residing in an intercellular bridge before abscission. Top left: about 1 μm to the right of the MB is the constriction zone. Top right: enlargement of inset in the top left panel, showing 'ripple contours' before abscission. Bottom: the right four images are from serial sections, showing the helical filaments that account for the appearance of ripple contours and that disappear on depletion of ESCRT-III components. Images of immunostained MBs (a) provided by courtesy of C-T. Chen and S.D. Electron micrographs (a,b) were reproduced, with permission, from [7,16].

retention or degradation [3,19,22,23]. Alternatively, the cell can sever the tether, releasing the post-mitotic MB it into the extracellular space [7,9,18,19], where it remains or is engulfed by a cell [16,19,22]. Retention, release, or degradation of post-mitotic MBs appears to depend on cell type and status [19,22,23]. These findings indicate that fate determination of post-mitotic MBs involves multiple steps, is likely to be tightly regulated (see below and [19,22,23]), and is far different from their fate as remnants or residual bodies, as proposed decades ago [16].

## The MB as an important platform for abscission

Renewed interest in MB research over the past decade revealed the extraordinary complexity of this organelle through proteomic analysis [43] and led to the discovery of myriad molecules and pathways that contribute to abscission. Previously known functions of these pathways in other cellular processes helped generate hypotheses to test for mechanisms of abscission. These pathways include vesicle trafficking, membrane scission, MT severing, and ubiquitination. Because many recent reviews cover mechanisms of abscission, we focus on how these pathways may contribute to MB retention by or release from cells.

### *Membrane trafficking pathways are targeted to the MB for abscission*

It is no surprise that multiple membrane trafficking pathways are crucial for abscission (for reviews, see [2,4,5]), because early EM studies identified many types of vesicle around the MB during early cytokinesis and before abscission. Recent studies showed that molecules involved in secretion and endocytosis were concentrated in the MB region during late cytokinesis [42,44,45]. Post-Golgi vesicles and proteins required for vesicle tethering (e.g., exocysts; see Glossary) and fusion (e.g., soluble N-ethylmaleimide-sensitive factor [NSF] attachment protein receptors [SNAREs]; see Glossary) were recruited to the MB [3,45–47] and this recruitment depended on centrosome/MB proteins (e.g., centriolin and CEP55; [3,13]). Disturbing either the localization or the function of these MB proteins or the recruitment of molecules required for secretion caused abscission failure. This resulted in a dramatic collapse of the intercellular bridge, creating binucleated cells [13,46], long delays in abscission, or multicellular syncytia formation [3,15]. These results clearly demonstrate the importance of selective secretion in abscission.

The endosomal pathway also contributes to abscission (for review, see [4]). As shown previously, the endosome-associated Rab11-interacting proteins FIP3 and FIP4 were targeted to the MB [42,46] and interacted with the exocyst component Exo70 and the MB protein mgcRacGAP/Cyk4 [46,48]. These interactions were essential for completing cytokinesis. These results indicate that the MB may serve as an anchoring scaffold for molecules and complexes that facilitate vesicle accumulation at or near this site and potentiate vesicle fusion during abscission. Alternatively, fusion of recruited secretory and endosomal vesicles may be required for elongating the intercellular bridge during late cytokinesis [25,26], for narrowing the bridge caliber (see above), or for preparing the site in other ways for the final separation step of abscission.

As shown previously, vesicles appeared to be targeted asymmetrically to one side of the MB before abscission [3]. This observation was consistent with the reported asymmetric accumulation of Golgi-derived vesicles at the MB during late cytokinesis, following their initial symmetric accumulation at both sides of the MB [21]. With better temporal resolution, the recruited Golgi-derived vesicles appeared to dock at the MB and remain individually without fusing [21], suggesting that these tethered vesicles were awaiting a signal to initiate vesicle fusion and abscission [3]. Conceptually similar was the work showing that the Golgi complex was organized in two positions in each nascent daughter cell during abscission [49]. The two major Golgi complexes were far away from the bridge, behind the nuclei of both nascent daughter cells near the centrosomes. The two minor pools of Golgi-derived membranes were located at the juncture of the intercellular bridge. In one of the two daughter cells, the minor Golgi-derived membrane pool was retracted back to the major site during late cytokinesis, leaving the minor pool of the other daughter cell in a position to deliver Golgi-derived membranes to one side of the MB to mediate abscission. Although FIP3/4-positive endosomes are trafficked symmetrically to the MB [42], more recent EM data suggests that they may not fuse until localized MT severing occurs asymmetrically on one side of the MB [40]. These new EM tomographic images leave room for the idea that fusion of endosomal vesicles may occur asymmetrically or sequentially, although their recruitment is symmetric. This observation also suggests a potential link between vesicle fusion and MT severing during abscission.

Thus, broadly speaking, regardless of how vesicles are recruited (e.g., symmetrically, asymmetrically, or sequentially), fusion events may still be 'asymmetric' or 'sequential', presumably due to limiting factors on one side of the MB or to sequential arrival at this site [21,40]. The consequence of these asymmetric or sequential events would be inheritance of the post-mitotic MB by one of the two daughter cells [3,21] or release after the bridge is severed, again on other side of the MB (discussed below). How these asymmetric or sequential events might contribute to MB retention or release is postulated in Box 3.

### *ESCRT complexes build helical filaments during abscission*

The recent finding that ESCRT is an evolutionarily conserved pathway required for abscission provides insight into a late step in this process [7,8,50–53]. ESCRT has important roles in the constriction of membranes during budding of viruses and vesicles (for reviews, see [54–56]). The topology of an enveloped virus budding from a host cell is similar to the intercellular bridge connecting one daughter cell with its sister before abscission. Severing the bridge to disconnect daughter cells is analogous to virus release from the cell and may require identical or similar functions of ESCRT (for reviews, see [5,56]). As predicted by the model, multiple ESCRT components (e.g., Alix and Tsg101) are targeted to the MB for abscission [8,50,57]. However, more recent studies led to a different model [7,9], where ESCRT-III components (e.g., CHMP2 and CHMP4A/B) appeared to localize to the MR initially, then, at a later time localized at a

**Box 3. Proposed mechanisms for asymmetric inheritance of post-mitotic MBs**

*Asymmetric vesicle trafficking → asymmetric abscission → MB retention by one daughter cell*

One model for asymmetric inheritance of post-mitotic MBs is that vesicles are recruited asymmetrically from one side of the MB for abscission and/or ESCRT follows. The bridge is then severed, resulting in MB inheritance to the opposing daughter cell. One example is the post-Golgi secretory vesicles labeled by luminal-GFP [3]. Given that other recycling endosomal vesicles have been observed to symmetrically traffic to the MB, we have compared the timing of luminal-GFP recruitment and the transport of FIP3- or Rab11-decorated endosomes to the MB. Luminal-GFP vesicles trafficked to the MB significantly later than FIP3 and Rab11 vesicles (Rosa and Doxsey, unpublished), suggesting that the asymmetric delivery of secretory vesicles is more likely to contribute to abscission, affecting where the post-mitotic MB ultimately resides. In another study, Golgi-derived membranes initially trafficked symmetrically to the MB, but later became asymmetrically localized before abscission [21]. These observations suggest that different vesicles may function at different times and traffic in different ways during abscission. Therefore, experiments should be normalized to a given end point, such as time pre-abscission, to reliably compare contributions of different classes of vesicles and results from different investigators.

*Symmetric vesicle trafficking → stochastic abscission → MB retention or release*

If vesicle trafficking and membrane scission machinery concentrate at both sides of the MB and cut the bridge sequentially rather than simultaneously, a post-mitotic MB can still be retained. Ultimately, the bridge on both sides of the MB could be severed by ESCRT, as recently suggested [7,9], and then released [19]. This appears to be the case for cells in which post-mitotic MBs are released extracellularly [17–19]. Time-lapse imaging and ultrastructural analysis revealed that these post-mitotic MBs remain connected to one daughter cell by a thin stalk for an extended time before they are eventually severed [18,19], suggesting that the abscission machinery takes longer to cleave on one side of the MB than the other. These observations reinforce the idea that, despite symmetric vesicle trafficking, severing capability (presumably the activity of the abscission machinery) on the two sides of the MB may be different, leading to asymmetric MB inheritance and, potentially, later MB release.

*Asymmetric signaling → asymmetric abscission → MB retention by one daughter cell*

The third model predicts that membrane fusion is a regulated process that occurs on only one side of the MB despite vesicle delivery to both sides. The regulation of membrane fusion/scission and abscission could be through asymmetric removal of limiting factors (e.g., MT bundles; [40]), the recruitment of fusion activators (e.g., kinase), or stimulation of a previously positioned activator by other means (e.g., $Ca^{2+}$ release) as in regulated secretion; for example, insulin granule secretion (for review, see [72]).

Combinations of these models are also possible. For example, triggers of membrane fusion/scission for abscission could be recruited asymmetrically to the MB or sequentially to either side of the MB, as proposed in the second possibility, or activated asymmetrically, as proposed in the third possibility.

secondary site corresponding to the constriction zone [7,9]. Depletion of CHMP2, the core component of ESCRT-III, led to the disappearance of the ripple contours and the spiral-shaped filaments [7], suggesting that ESCRT-III contributes to their assembly. However, it was unclear whether ripples alone or both ripples and the constriction zone were lost on CHMP2 depletion and this could lead to a different interpretation of how ESCRT functions at these sites. Besides building filaments, ESCRT has been shown to interact with spastin [58], a AAA+ ATPase that severs MTs, providing a model where ESCRT function is coordinated with MT severing during abscission.

Several issues with the ESCRT model require further clarification. Although the Archaea ESCRT machinery spans the division site, which is approximately 1 μm in diameter at the beginning of cell fission (for review, see [59]), ESCRT-deformed membranes identified in eukaryotic cells typically have diameters of 50–100 nm [54–56]. These diameters are still significantly smaller than the diameter of the constriction zone at the intercellular bridge (200–500 nm) [3,7,9,16], so it is unclear how ESCRT forms filaments within the intercellular bridge and whether they are functionally capable of inducing bridge severing. One potential model, as discussed above, is that vesicles and fusion machinery, which are organized in a topologically different manner from ESCRT, are recruited to the MB where they contribute to bridge remodeling and narrowing, thus allowing ESCRT to function in the later stages of abscission. Alternatively, ESCRT itself may extrude membrane and cytoplasm into the extracellular environment to narrow the bridge caliber through a mechanism similar to viral budding before the final cut of the bridge, as observed in some EM studies [16,18,28]. Another model is that vesicle trafficking and ESCRT machinery work together to accomplish abscission, because both are increasingly recruited to the MB and the constriction zone at least 10 min before bridge severing [3,9,21]. In short, it remains unclear how vesicles, fusion machinery, and ESCRT remodel and/or sever the bridge membrane in a concordant manner.

More questions remain about the ESCRT model. How is ESCRT-III directed to the constriction zone? ESCRT-III spirals may grow from the MB where other ESCRT components reside, becoming increasingly smaller in diameter as they approach the constriction zone, approximately 1 μm distal to the MB. In a similar context, it is unknown whether recruitment of ESCRT-III and the appearance of ripple contours at the constriction zone require the prior presence of ESCRT-I or ESCRT-associated proteins at the MB, although depletion of these ESCRT components results in abscission failure. It is also unclear whether ESCRT functions together with regulated disassembly of cortical actin by F-actin modulators during abscission. Contradictory data suggest that ESCRT functions alone in abscission [7] or, alternatively, that ESCRT acts only at certain stages of abscission before 'secondary constriction', where fusion of FIP3 endosomes and disassembly of F-actin contribute to the final separation [60]. These questions may be answered by live imaging of F-actin and ESCRT-III components tagged with photo-distinguishable tags or by ultrastructural analysis of the constriction zone after selective depletion of ESCRT-I components and ESCRT-associated proteins. Despite these remaining questions, it is clear that the ESCRT pathway is crucial for abscission.

### *Role of deubiquitination/ubiquitination in modifying the MB on abscission*

In line with the ESCRT model of abscission, it was shown that two ESCRT-modulating deubiquitinating enzymes

(DUBs), UBPY/USP8 and AMSH, were recruited to the MB during cytokinesis [11]. Depletion of either DUB led to cytokinesis failure. AMSH depletion induced binucleated cells and cells interconnected by long bridges and UBPY depletion induced binucleated cells. This phenotypic difference may reflect different specificities of the two DUBs toward different MB protein substrates and ubiquitin conjugates [11,61,62]. The spatial distribution of UBPY and AMSH were different from anaphase to cytokinesis, suggesting selective interactions with different ESCRT and non-ESCRT molecules, which could be crucial for ordered abscission. The role of ubiquitin-mediated modifications in abscission is supported by work showing that BRUCE, a giant protein possessing E2/E3 ubiquitin ligase activity, moved to the MB, interacted with MB components, such as mitotic kinesin-like protein 1 (Mklp1), and blocked abscission when depleted [10]. The MB fraction of both BRUCE and Mklp1 were heavily mono- or oligo-ubiquitinated on abscission and both proteins appeared to be targeted by UBPY [10]. Taken together, ubiquitinating enzymes and ESCRT-interacting DUBs modulate the ubiquitination status of MB proteins, which may play a role in abscission and fate determination of post-abscission MBs (see below).

## Multiple pathways control the fate of post-mitotic MBs

### *Intracellular degradation via macroautophagy*

One of the intriguing discoveries regarding the fate of post-mitotic MBs is the role of macroautophagy (hereafter referred to as autophagy) [19,22,23]. As reviewed previously, autophagy contributes to the recycling of amino acids, embryonic development, and disease pathogenesis [63,64]. Autophagy can be selective and mediated by autophagic receptors. Receptor recognition is followed by autophagosome formation, autophagosome fusion with lysosomes, and degradation of encapsulated organelles or proteins [65]. The NBR1 autophagic receptor was shown to play a dominant role in degradation of post-mitotic MBs through its recognition of CEP55, a core MB component crucial for abscission; another receptor, p62, was also implicated in this process [22,23]. Besides receptor recognition, the level of autolysosomal activity can affect the degradation efficiency of post-mitotic MBs [22]. Taking these findings together, autophagy is a major contributor to MB clearance.

### *MB release from cells*

As shown by early EM studies, an alternative fate of the post-mitotic MB was release into the extracellular space [16]. Using bone marrow-derived cells *in vitro*, extracellular, and partially deteriorated, MBs were observed [16]. The first evidence for MB release *in vivo* came from the finding of electron-dense particles inside the lumen of the neural tube of mouse embryos, although these particles were not initially recognized as released MBs [17]. In subsequent studies, time-lapse imaging and EM demonstrated that MBs were released from neural precursor cells *in vivo* not only in mice, but also in chicken [18] and from mouse neural stem cells *in vitro* [19]. Interestingly, released MBs collected in mouse ventricular fluid increased significantly at the early stages of neurogenesis (E10.5–12.5) [17], coincident with the time when differentiating (neurogenic) divisions become prominent [17,66]. This suggested that MB release might depend on cell type/status and could contribute to these states. Depletion of the ESCRT-associated protein Alix reduced the amount of free MBs in the medium of neural stem cells (NS-5) and neuroblastoma cells (Neuro-2a), suggesting that MB release was likely to involve the secondary scission event at the tether between the MB and the daughter cell [19]. It is also possible that Alix depletion might affect the first scission event between the two nascent daughters, leading to binucleated cell formation. However, this was not observed in the aforementioned cells [19], maybe because the role of Alix in abscission was minor or slightly different in these two cell types. MB release is clearly a dominant feature of certain cell types and appears to be dependent on culture conditions *in vitro* or the developmental or differentiation state of cells *in vivo* (discussed below; [19,22]).

### *Alternative routes that lead to MB clearance*

MB release and autophagic degradation of MBs are most likely to represent parallel pathways for MB clearance [16,19,22,23]. HeLa cells and mouse Neuro-2a cells can degrade MBs by autophagy and release them into the extracellular space [19,22,23], demonstrating that both pathways can be used in a single cell and suggesting interplay between these pathways. Because MB fate has not been characterized in great detail until recently, it is reasonable to envision additional routes for MB clearance that ultimately lead to intracellular degradation or release from cells. In fact, recent ultrastructural analysis of post-mitotic MBs revealed characteristics different from mitotic MBs (e.g., fewer or no MTs), presumably due to MB aging [18,19]. These morphological changes could represent the products of different resident times in autolysosomes or products of pre-autophagic events that change post-mitotic MB integrity and composition. It is also possible that long after release from cells, post-mitotic MBs are internalized by endocytosis/phagocytosis followed by heterolysosomal or autophagic degradation [19]. These different yet not mutually exclusive routes may all exist, but they are difficult to distinguish. It is also difficult to know whether the same autophagy machinery is required as a final step for all of these routes. Nevertheless, the temporal analysis of MB degradation [22] and the ultrastructural analysis of post-mitotic MBs [19] shed light on when and how MBs are destined for intracellular degradation. Additional studies are required to more closely track the degradation process and test how different degradation pathways are utilized by different cells.

### *Pathways for MB clearance in different cell types: consensus and dissensus*

In the grand scheme, increasing the activities of either or both autophagy and MB release can promote MB clearance when MBs generated during proliferation need to be removed. One such scenario is differentiation [19,22]. In this context, cells derived from different developmental lineages or with different pluripotency status may employ one or both pathways for MB clearance, depending on the environment and what is available in the toolbox. Therefore, differentiating cells may promote MB clearance either

by elevating autophagic activity, as observed in fibroblasts derived from human embryonic stem cells (hESCs) [19,22,23], or by enhancing MB release (NS-5 and Neuro-2a) [19] to achieve the same goal, the elimination of MBs.

The aforementioned model does not necessarily imply low MB release in undifferentiated cells, such as multi/oligopotent stem cells. In fact, significant basal levels of MB release have been observed in neural progenitors *in vivo* and neural stem cells *in vitro*, although the levels increase further during the early stages of neurogenesis (differentiation) *in vivo* and during induced neuronal differentiation [17–19]. However, we currently do not know whether constitutively high MB release is also a characteristic of hESCs (e.g., H1, H9) and induced pluripotent stem cells (iPSCs) or whether pluripotency status (e.g., pluripotency versus oligo/unipotency) or developmental lineage influences MB clearance. Nevertheless, it was agreed in the two recent studies that autophagy plays little to no role in the fate determination of post-mitotic MBs in embryonic and neural stem cells [19,22]; although it is unclear whether this is due to the low autophagic activity of this cell type or high MB release.

Another question arising from these studies is how to interpret the variability of MB retention and release across multiple cancer-derived cell lines. *A priori*, the genomic instability in such cells makes it difficult to evaluate results between different cell lines. It was shown that neural stem cells had a high basal level of MB release (90% of the MBs after abscission), whereas neuroblastoma cells and other cancer cells had only a medium to low level of release (10–50%) [19]. It was proposed that cancer cells exploit autophagy for MB clearance, which is consistent with what was shown recently [22]. One problem with the interpretation of the data from these two studies is that each was focused on a different cellular process and for the most part on different cell types. What is needed is a study designed to examine both degradation and release of MBs in the same panel of cell types *in vivo* and *in vitro*. Under the same experimental conditions, one could better understand the contributions of autophagic degradation, MB release, and possibly other pathways to MB fate determination in cell types with low to high pluripotency.

## Emerging non-cytokinetic roles of MBs

Not until recently have researchers begun to study the fate of MBs after cytokinesis [18,19,22,23]. The few studies completed thus far suggest that MBs may have non-cytokinetic functions, such as polarity specification [67,68], intercellular communication [17,18], and cell fate determination [19,22]. This is intriguingly analogous to studies showing multifunctionality of other structural assemblies generated during cytokinesis, such as bud scars in yeast and cytokinesis or cell-division remnants in nematodes. In addition to the cytokinetic roles of these assemblies, they also define polarity for the upcoming cell division (Box 4).

Post-mitotic MBs have also been implicated in cell polarity. In the fly notum and chick spinal cord, post-mitotic MBs of neurons were found at the polarized/apical domain where the future neurite or apical process sprouted [67,68]. This led to the model that post-mitotic MBs might specify neuronal polarity. Post-mitotic MBs have also been implicated in intercellular communication, presumably to maintain the balance between differentiating cells and progenitors [17]. This idea is based on the fact that MB release into the ventricle lumen increases significantly after neurogenesis [17,18]. One of the candidates for delivering such intercellular signals is Prominin-1 (CD133), a

**Box 4. Bud scars, cytokinesis remnants, cell-division remnants, and post-mitotic MBs**

MBs are formed between dividing cells and appear to have additional non-cytokinetic roles, as recently revealed (this review; [19,22,67,68]). Similar structural assemblies formed during cytokinesis are also observed in unicellular organisms, such as yeast (for review, see [73]). Although the molecular composition of these structural assemblies, namely bud scars, differs from that of MBs, their ring-like morphology is surprisingly similar [74,75]. In addition to their cytokinetic roles, it is important to note that bud scars appear to send prohibitory signals to avoid repetitive budding at the same site in the next division cycle, but allow budding at abutted sites [75–77]. This function involves: (i) timely recruitment of multiple molecules to the bud neck region before cytokinesis is completed; and (ii) restrictive regulation of GTPase activity around the bud ([75,76]; for review, see [73]). These events contribute to cell polarity and defining the division axis for the next cell division. Thus, a post-mitotic scar in yeast also has additional non-cytokinetic roles.

In *Caenorhabditis elegans*, a 'cytokinesis remnant; is formed when cytokinesis is completed [78–80]. This structure was first identified as a membrane invagination enriched with F-actin and actin-capping proteins that remains at the anterior cortex of the posterior cell in two-cell embryos but does not seem to accumulate after multiple divisions [79,80]. In work in which different fixation conditions were used, multiple F-actin-enriched remnants were observed and the total number was one less than the number of divisions (e.g., seven remnants if eight divisions in total; [79]). These accumulating structures were thus named 'cell-division remnants', because it was unclear whether they are the same structures as cytokinesis remnants. Moreover, it is unclear whether these structures are MBs, because most metazoans' MBs are not F-actin enriched and the remnants have not been shown to contain *bone fide* MB components.

As shown previously, on completion of cytokinesis, a ring-like cytokinesis remnant surrounding the post-mitotic MB starts to form [78–80]. The spindle in the cell with a cytokinesis remnant rotates and aligns toward the cytokinesis remnant, where actin, actin-capping proteins, and dynein are enriched [78–82]. The alignment seems to require MTs, motors, and actin [78,81,83]. This newly formed cytokinesis remnant is the one that directs spindle alignment in the nematode embryo, just as the newest bud scar defines the cell division axis in yeast. Thus, the *C. elegans* cytokinesis remnant, the membrane domain surrounding the remnant, or both could have additional roles beyond cytokinesis.

It is unclear why different organisms, from unicellular to multicellular and from yeast to humans, have evolved or conserved a similar structural assembly that is used for cytokinesis then reused for other post-mitotic proposes, such as defining polarity *in vivo*. Of note, these structure assemblies appear to be compositionally different. What is the selective pressure driving formation of structurally similar but molecularly diverse organelles? For example, bud scars are mainly chitinous (for review, see [73]). Cytokinesis remnants are membrane invaginations enriched in dynein, actin, and actin-capping proteins. Metazoan MB derivatives are protein structures comprising multiple MB proteins, membranes, and MTs, but do not appear to be actin-enriched. Additional comparative analysis of the MB and its counterparts in other organisms is required to understand the roles of these related structures and to determine whether they have common functions beyond cytokinesis.

(cancer) stem cell marker and pentaspan membrane protein concentrated at the MB of neural progenitors (for review, see [69]). As neurogenesis proceeds, small Prominin-1-positive vesicles arise from decomposing released MBs and may participate in intercellular communication. These intriguing results nicely link post-mitotic MBs to polarity specification and intercellular signaling in the nervous system; however, more work is required to confirm these ideas and determine what molecules are involved.

In addition to these potential roles of post-mitotic MBs, it was recently shown that experimental manipulation of MB clearance can sensitize cells for cell fate conversion, including differentiation and reprogramming programs [19,22]. For example, inhibiting MB clearance/release could sensitize oligopotent neural progenitors to differentiate toward differentiated neurons. The opposite cell fate conversion, from terminally differentiated fibroblasts to iPSCs may be sensitized by inducing MB retention within cells [19,22]. This correlation between MB-low cells and differentiation status and MB-high cells and pluripotency status is an intriguing relationship that needs to be further analyzed to identify the role of MBs in these processes. Although the potential of MBs to drive cells toward both differentiation and pluripotency pathways may seem contradictory, it is plausible if the modulator, presumably the MB, is itself modified in different ways. The reciprocal conversion between stem cells and differentiated cells could potentially result from different signaling molecules harbored in post-mitotic MBs or, more simply, through the overall level of MBs in cells with different pluripotency status, from high (oligopotent) to low/none (differentiated cells). One must also consider as a contributing factor in cell fate conversion the different experimental manipulations used to modulate potency in the two studies (e.g., inhibiting MB degradation versus MB release). Despite these open questions, the role of post-mitotic MBs in cell fate conversion is clearly emerging. For example, increased MB retention in neural stem cells achieved by inhibiting MB release promotes cell fate conversion toward differentiation [19]. Increased MB retention in differentiated cells achieved by depleting the NBR1 autophagic receptor enhances cell fate conversion toward pluripotency [22]. Therefore, together with the other studies reviewed above, the idea that MBs possess multiple non-cytokinetic roles, unrelated to cell division, is becoming apparent. These new findings certainly require further investigation to tease out the molecular mechanisms and will in turn advance our understanding of (asymmetric) cell divisions in stem cell biology.

## Concluding remarks

For almost a century, the MB has been perceived simply as a link between two dividing daughter cells that was discarded after division. More recently, its role as an organizing site for abscission was proposed [3,8,12,13,21,42]. Moreover, based on the diversity of proteins associated with MBs identified in numerous studies and the 'MB parts list' obtained from mass spectrometry [43], additional functions of MBs and post-mitotic MBs will surely be uncovered over years to come.

As discussed above, data from many studies as well as suggestions from the MB proteome indicate that multiple pathways converge in the vicinity of the MB during abscission [3,6–9,21,42–45]. Although further clarification is needed on how these pathways mediate abscission, one must consider cooperative functioning of fusion and fission machinery, either consecutively or concordantly, as an essential part of this process. For example, vesicle fusion along the bridge to remodel the bridge membrane might set the stage allowing ESCRT to function or work concordantly with ESCRT to accomplish the ultimate membrane fission for abscission. We favor the latter model, given the similar timing of elevated vesicle trafficking to the bridge and ESCRT-III translocation to the constriction zone [3,9,21]. ESCRT may coordinate MT disassembly in the bridge by timed interaction with MT-severing proteins [58]. This coordination could be a critical factor during abscission. However, complete MT loss before abscission may not be required, given the considerable number of MT bundles that are retained by post-mitotic MBs following abscission [3,7].

The inheritance and retention of the post-mitotic MB by one daughter cell is remarkable and makes the two genetically identical daughter cells no longer equal. One inherits a large organelle comprising hundreds of proteins; the other receives no post-mitotic MBs. In parallel, post-mitotic MBs can be released, presumably to remove critical molecules from daughter cells. Although questions remain about the details, intriguing new evidence has begun to uncover the functional significance of post-mitotic MBs (see above). We are beginning to get glimpses of MBs as structures whose retention and loss can influence stem cells, cancer cells, and differentiated cells. The potential roles of MBs in influencing cell fate determination are unanticipated and exciting. Further investigation is required to understand precisely how these organelles impact cellular function. In any case, it is clear that the current perception of post-mitotic MBs has risen from remnants jettisoned from cells to post-mitotic organelles serving unexpected functions.

## References


1 Guizetti, J. and Gerlich, D.W. (2010) Cytokinetic abscission in animal cells. *Semin. Cell Dev. Biol.* 21, 909–916
2 Barr, F.A. and Gruneberg, U. (2007) Cytokinesis: placing and making the final cut. *Cell* 131, 847–860
3 Gromley, A. *et al.* (2005) Centriolin anchoring of exocyst and SNARE complexes at the midbody is required for secretory-vesicle-mediated abscission. *Cell* 123, 75–87
4 Prekeris, R. and Gould, G.W. (2008) Breaking up is hard to do - membrane traffic in cytokinesis. *J. Cell Sci.* 121, 1569–1576
5 Caballe, A. and Martin-Serrano, J. (2011) ESCRT machinery and cytokinesis: the road to daughter cell separation. *Traffic* 12, 1318–1326
6 Connell, J.W. *et al.* (2009) Spastin couples microtubule severing to membrane traffic in completion of cytokinesis and secretion. *Traffic* 10, 42–56
7 Guizetti, J. *et al.* (2011) Cortical constriction during abscission involves helices of ESCRT-III-dependent filaments. *Science* 331, 1616–1620
8 Carlton, J.G. and Martin-Serrano, J. (2007) Parallels between cytokinesis and retroviral budding: a role for the ESCRT machinery. *Science* 316, 1908–1912
9 Elia, N. *et al.* (2011) Dynamics of endosomal sorting complex required for transport (ESCRT) machinery during cytokinesis and its role in abscission. *Proc. Natl. Acad. Sci. U.S.A.* 108, 4846–4851
10 Pohl, C. and Jentsch, S. (2008) Final stages of cytokinesis and midbody ring formation are controlled by BRUCE. *Cell* 132, 832–845
11 Mukai, A. *et al.* (2008) Dynamic regulation of ubiquitylation and deubiquitylation at the central spindle during cytokinesis. *J. Cell Sci.* 121, 1325–1333

12 Fabbro, M. *et al.* (2005) Cdk1/Erk2- and Plk1-dependent phosphorylation of a centrosome protein, Cep55, is required for its recruitment to midbody and cytokinesis. *Dev. Cell* 9, 477–488
13 Zhao, W.M. *et al.* (2006) Cep55, a microtubule-bundling protein, associates with centralspindlin to control the midbody integrity and cell abscission during cytokinesis. *Mol. Biol. Cell* 17, 3881–3896
14 Ganem, N.J. *et al.* (2007) Tetraploidy, aneuploidy and cancer. *Curr. Opin. Genet. Dev.* 17, 157–162
15 Gromley, A. *et al.* (2003) A novel human protein of the maternal centriole is required for the final stages of cytokinesis and entry into S phase. *J. Cell Biol.* 161, 535–545
16 Mullins, J.M. and Biesele, J.J. (1977) Terminal phase of cytokinesis in D-98s cells. *J. Cell Biol.* 73, 672–684
17 Marzesco, A.M. *et al.* (2005) Release of extracellular membrane particles carrying the stem cell marker prominin-1 (CD133) from neural progenitors and other epithelial cells. *J. Cell Sci.* 118, 2849–2858
18 Dubreuil, V. *et al.* (2007) Midbody and primary cilium of neural progenitors release extracellular membrane particles enriched in the stem cell marker prominin-1. *J. Cell Biol.* 176, 483–495
19 Ettinger, A.W. *et al.* (2011) Proliferating versus differentiating stem and cancer cells exhibit distinct midbody-release behaviour. *Nat. Commun.* 2, 503
20 Jantsch-Plunger, V. *et al.* (2000) CYK-4: A Rho family gtpase activating protein (GAP) required for central spindle formation and cytokinesis. *J. Cell Biol.* 149, 1391–1404
21 Goss, J.W. and Toomre, D.K. (2008) Both daughter cells traffic and exocytose membrane at the cleavage furrow during mammalian cytokinesis. *J. Cell Biol.* 181, 1047–1054
22 Kuo, T.C. *et al.* (2011) Midbody accumulation through evasion of autophagy contributes to cellular reprogramming and tumorigenicity. *Nat. Cell Biol.* 13, 1214–1223
23 Pohl, C. and Jentsch, S. (2009) Midbody ring disposal by autophagy is a post-abscission event of cytokinesis. *Nat. Cell Biol.* 11, 65–70
24 Flemming, W. (1891) Neue Beiträge zur Kenntnis der Zelle. *Arch. Mikrosk. Anat.* 37, 685–751 (in German)
25 Mullins, J.M. and Biesele, J.J. (1973) Cytokinetic activities in a human cell line: the midbody and intercellular bridge. *Tissue Cell* 5, 47–61
26 Byers, B. and Abramson, D.H. (1968) Cytokinesis in HeLa: post-telophase delay and microtubule-associated motility. *Protoplasma* 66, 413–435
27 Buck, R.C. and Tidsale, J.M. (1962) An electron microscopic study of the cleavage furrow in mammalian cells. *J. Cell Biol.* 13, 117–125
28 Buck, R.C. and Tisdale, J.M. (1962) The fine structure of the mid-body of the rat erythroblast. *J. Cell Biol.* 13, 109–115
29 Jones, O.P. (1969) Elimination of midbodies from mitotic erythroblasts and their contribution to fetal blood plasma. *J. Natl. Cancer. Inst.* 42, 753–759
30 Robbins, E. and Gonatas, N.K. (1964) The ultrastructure of a mammalian cell during the mitotic cycle. *J. Cell Biol.* 21, 429–463
31 Paweletz, N. (1967) On the function of the "Flemming body" during division of animal cells. *Naturwissenschaften* 54, 533–535
32 Moll, E. and Paweletz, N. (1980) Membranes of the mitotic apparatus of mammalian cells. *Eur. J. Cell Biol.* 21, 280–287
33 Brinkley, B.R. and Cartwright, J., Jr (1971) Ultrastructural analysis of mitotic spindle elongation in mammalian cells in vitro. Direct microtubule counts. *J. Cell Biol.* 50, 416–431
34 Hepler, P.K. and Jackson, W.T. (1968) Microtubules and early stages of cell-plate formation in the endosperm of *Haemanthus katherinae* Baker. *J. Cell Biol.* 38, 437–446
35 Otegui, M.S. *et al.* (2005) Midbodies and phragmoplasts: analogous structures involved in cytokinesis. *Trends Cell Biol.* 15, 404–413
36 Sanger, J.M. *et al.* (1985) Midbody sealing after cytokinesis in embryos of the sea urchin *Arabacia punctulata*. *Cell Tissue Res.* 240, 287–292
37 Schmidt, K. and Nichols, B.J. (2004) A barrier to lateral diffusion in the cleavage furrow of dividing mammalian cells. *Curr. Biol.* 14, 1002–1006
38 Steigemann, P. *et al.* (2009) Aurora B-mediated abscission checkpoint protects against tetraploidization. *Cell* 136, 473–484
39 McIntosh, J.R. and Landis, S.C. (1971) The distribution of spindle microtubules during mitosis in cultured human cells. *J. Cell Biol.* 49, 468–497
40 Schiel, J.A. *et al.* (2011) Endocytic membrane fusion and buckling-induced microtubule severing mediate cell abscission. *J. Cell Sci.* 124, 1411–1424
41 Elad, N. *et al.* (2011) Microtubule organization in the final stages of cytokinesis as revealed by cryo-electron tomography. *J. Cell Sci.* 124, 207–215
42 Wilson, G.M. *et al.* (2005) The FIP3-Rab11 protein complex regulates recycling endosome targeting to the cleavage furrow during late cytokinesis. *Mol. Biol. Cell* 16, 849–860
43 Skop, A.R. *et al.* (2004) Dissection of the mammalian midbody proteome reveals conserved cytokinesis mechanisms. *Science* 305, 61–66
44 Skop, A.R. *et al.* (2001) Completion of cytokinesis in *C. elegans* requires a brefeldin A-sensitive membrane accumulation at the cleavage furrow apex. *Curr. Biol.* 11, 735–746
45 Low, S.H. *et al.* (2003) Syntaxin 2 and endobrevin are required for the terminal step of cytokinesis in mammalian cells. *Dev. Cell* 4, 753–759
46 Fielding, A.B. *et al.* (2005) Rab11-FIP3 and FIP4 interact with Arf6 and the exocyst to control membrane traffic in cytokinesis. *EMBO J.* 24, 3389–3399
47 Cascone, I. *et al.* (2008) Distinct roles of RalA and RalB in the progression of cytokinesis are supported by distinct RalGEFs. *EMBO J.* 27, 2375–2387
48 Simon, G.C. *et al.* (2008) Sequential Cyk-4 binding to ECT2 and FIP3 regulates cleavage furrow ingression and abscission during cytokinesis. *EMBO J.* 27, 1791–1803
49 Gaietta, G.M. *et al.* (2006) Golgi twins in late mitosis revealed by genetically encoded tags for live cell imaging and correlated electron microscopy. *Proc. Natl. Acad. Sci. U.S.A.* 103, 17777–17782
50 Morita, E. *et al.* (2007) Human ESCRT and ALIX proteins interact with proteins of the midbody and function in cytokinesis. *EMBO J.* 26, 4215–4227
51 Carlton, J.G. *et al.* (2008) Differential requirements for Alix and ESCRT-III in cytokinesis and HIV-1 release. *Proc. Natl. Acad. Sci. U.S.A.* 105, 10541–10546
52 Samson, R.Y. *et al.* (2008) A role for the ESCRT system in cell division in Archaea. *Science* 322, 1710–1713
53 Spitzer, C. *et al.* (2006) The *Arabidopsis* elch mutant reveals functions of an ESCRT component in cytokinesis. *Development* 133, 4679–4689
54 Raiborg, C. and Stenmark, H. (2009) The ESCRT machinery in endosomal sorting of ubiquitylated membrane proteins. *Nature* 458, 445–452
55 McDonald, B. and Martin-Serrano, J. (2009) No strings attached: the ESCRT machinery in viral budding and cytokinesis. *J. Cell Sci.* 122, 2167–2177
56 Wollert, T. *et al.* (2009) The ESCRT machinery at a glance. *J. Cell Sci.* 122, 2163–2166
57 Lee, H.H. *et al.* (2008) Midbody targeting of the ESCRT machinery by a noncanonical coiled coil in CEP55. *Science* 322, 576–580
58 Yang, D. *et al.* (2008) Structural basis for midbody targeting of spastin by the ESCRT-III protein CHMP1B. *Nat. Struct. Mol. Biol.* 15, 1278–1286
59 Samson, R.Y. and Bell, S.D. (2009) Ancient ESCRTs and the evolution of binary fission. *Trends Microbiol.* 17, 507–513
60 Schiel, J.A. *et al.* (2012) FIP3-endosome-dependent formation of the secondary ingression mediates ESCRT-III recruitment during cytokinesis. *Nat. Cell Biol.* 14, 1068–1078
61 Mizuno, E. *et al.* (2006) A deubiquitinating enzyme UBPY regulates the level of protein ubiquitination on endosomes. *Traffic* 7, 1017–1031
62 Row, P.E. *et al.* (2007) The MIT domain of UBPY constitutes a CHMP binding and endosomal localization signal required for efficient epidermal growth factor receptor degradation. *J. Biol. Chem.* 282, 30929–30937
63 Cecconi, F. and Levine, B. (2008) The role of autophagy in mammalian development: cell makeover rather than cell death. *Dev. Cell* 15, 344–357
64 Levine, B. and Kroemer, G. (2008) Autophagy in the pathogenesis of disease. *Cell* 132, 27–42
65 Klionsky, D.J. (2007) Autophagy: from phenomenology to molecular understanding in less than a decade. *Nat. Rev. Mol. Cell Biol.* 8, 931–937
66 Kosodo, Y. *et al.* (2004) Asymmetric distribution of the apical plasma membrane during neurogenic divisions of mammalian neuroepithelial cells. *EMBO J.* 23, 2314–2324
67 Wilcock, A.C. *et al.* (2007) Mitotic spindle orientation distinguishes stem cell and terminal modes of neuron production in the early spinal cord. *Development* 134, 1943–1954

68 Pollarolo, G. *et al.* (2011) Cytokinesis remnants define first neuronal asymmetry in vivo. *Nat. Neurosci.* 14, 1525–1533
69 Corbeil, D. *et al.* (2010) Prominin-1: a distinct cholesterol-binding membrane protein and the organisation of the apical plasma membrane of epithelial cells. *Subcell. Biochem.* 51, 399–423
70 Jurgens, G. (2005) Plant cytokinesis: fission by fusion. *Trends Cell Biol.* 15, 277–283
71 Allenspach, A.L. and Roth, L.E. (1967) Structural variations during mitosis in the chick embryo. *J. Cell Biol.* 33, 179–196
72 Pickett, J.A. and Edwardson, J.M. (2006) Compound exocytosis: mechanisms and functional significance. *Traffic* 7, 109–116
73 Bi, E. and Park, H.O. (2012) Cell polarization and cytokinesis in budding yeast. *Genetics* 191, 347–387
74 Chant, J. and Pringle, J.R. (1995) Patterns of bud-site selection in the yeast *Saccharomyces cerevisiae*. *J. Cell Biol.* 129, 751–765
75 Tong, Z. *et al.* (2007) Adjacent positioning of cellular structures enabled by a Cdc42 GTPase-activating protein-mediated zone of inhibition. *J. Cell Biol.* 179, 1375–1384
76 Marston, A.L. *et al.* (2001) A localized GTPase exchange factor, Bud5, determines the orientation of division axes in yeast. *Curr. Biol.* 11, 803–807
77 Halme, A. *et al.* (1996) Bud10p directs axial cell polarization in budding yeast and resembles a transmembrane receptor. *Curr. Biol.* 6, 570–579
78 Hyman, A.A. (1989) Centrosome movement in the early divisions of *Caenorhabditis elegans*: a cortical site determining centrosome position. *J. Cell Biol.* 109, 1185–1193
79 Waddle, J.A. *et al.* (1994) Transient localized accumulation of actin in *Caenorhabditis elegans* blastomeres with oriented asymmetric divisions. *Development* 120, 2317–2328
80 Keating, H.H. and White, J.G. (1998) Centrosome dynamics in early embryos of *Caenorhabditis elegans*. *J. Cell Sci.* 111, 3027–3033
81 Skop, A.R. and White, J.G. (1998) The dynactin complex is required for cleavage plane specification in early *Caenorhabditis elegans* embryos. *Curr. Biol.* 8, 1110–1116
82 Pichler, S. *et al.* (2000) OOC-3, a novel putative transmembrane protein required for establishment of cortical domains and spindle orientation in the P(1) blastomere of *C. elegans* embryos. *Development* 127, 2063–2073
83 Hyman, A.A. and White, J.G. (1987) Determination of cell division axes in the early embryogenesis of *Caenorhabditis elegans*. *J. Cell Biol.* 105, 2123–2135